Graph State Properties and Applications in the Stabilizer Formalism

Alice R. Cullen
Supervisor: Prof. Pieter Kok

Submitted for the Degree of Doctor of Philosophy

School of Mathematical and Physical Sciences
The University of Sheffield

Abstract

Graph states form a class of entangled quantum states that have multiple useful applications within quantum computing and quantum communication protocols. The stabilizer formalism offers an efficient mathematical description of graph states and the effect of operations acting on such states. Here, we consider three scenarios where the stabilizer formalism can be utilised to investigate the structure, manipulation and generation of graph states. First, we propose a method to calculate the purity of reduced states of graph states entirely within the stabilizer formalism, using only the stabilizer generators for a given state and apply this method to find the Concentratable Entanglement of graph states. Next, we reduce the number of qubits required within a graph state used as a resource for the measurement based implementation of a general two-qubit unitary, using the stabilizer formalism to track supplementary operations that are required. Finally, we examine spin-photon interactions followed by single-qubit measurements as a process to probabilistically generate states described by the stabilizer formalism, particularly when the phase shift induced is small.

Acknowledgments

I would like to thank Pieter, my supervisor, for his guidance throughout my time at Sheffield. I appreciate all those within the physics department, LDSD group and E13a who have contributed to my PhD experience.

I am grateful to Cosmo Lupo (Politecnico di Bari) and Emilien Lavie, Molly Thomas, Imogen Forbes, Naomi Solomons and Patrick Yard of QET Labs (University of Bristol) for the invitation to work with them. It was also a pleasure to meet up at events they helped organise — the summer school on Quantum Optical Technologies in Trani, Italy and the workshop on Quantum Information Technologies in Bristol.

Finally thanks to my family: to my parents for their support, to Tom for all his encouragement and for moving to Sheffield, and to Barney, my dog, for being my work-from-home colleague.

Contents

Chapter 1

Introduction

1.1 Quantum Information

Quantum computers have the potential to perform specific tasks far more efficiently than their classical counterparts. For example, the Variational Quantum Eigensolver (VQE) [1, 2] is a quantum algorithm that provides a polynomial speed-up in finding the ground state of a system, Grover's algorithm [3] offers a quadratic speed-up in unstructured searches and Shor's algorithm [4] is exponentially faster in factoring integers than classical methods. Other quantum algorithms used within quantum machine learning [5] range from quadratic [6, 7] to exponential speed-ups [8, 9] over the best equivalent classical algorithms. Additionally, provably secure Quantum Key Distribution (QKD) algorithms [10, 11] rely solely on quantum mechanical properties rather than the sheer computational complexity of classical protocols. The concept of 'quantum supremacy' has been suggested [12], wherein it may be possible for quantum computers to solve problems that cannot be approached classically, however this is yet to be decisively demonstrated.

In the simplest case, a quantum computer can consist of a single quantum bit or qubit. This is any two-level quantum mechanical system where the state of the system can be either of the two possible states or in some superposition of them. The concept of superposition, in which a qubit can simultaneously be in more than one state is an entirely quantum property and is one of the contributing factors to the additional 'power' of a quantum computer. A computation can be performed by applying quantum operations or gates to the qubit and by measuring the state of the qubit. To enact more complex quantum computations, a quantum computer may consist of multiple qubits that undergo quantum gates and measurements. Further, these qubits may be prepared in such a way that they are said to be entangled [13, 14], where the state of an individual qubit is dependent on the state of the other entangled qubits, even when there is spatial separation. This quantum

phenomenon of entanglement is an additional provider of the time and security advantages that quantum computers can provide over classical computers.

One proposed implementation of quantum computing is via the one-way quantum computer [15, 16], which consists of a lattice-like structure of entangled qubits, and is capable of performing quantum circuits and algorithms via measurements of individual qubits within the lattice in a process known as Measurement Based Quantum Computing (MBQC). The states of entangled qubits belong to a class of quantum states known as graph states [17], which are an important resource within many quantum computing procedures.

Rather than operating quantum computers in isolation, quantum networks aim to connect multiple quantum computers to establish communication channels capable of transmitting quantum information. In time, this could provide a quantum internet [18, 19] on a global scale with the aid of technologies such as quantum satellites [20]. For practical, real-world communication, the distance quantum information must be shared across is of the order of thousands of kilometres. Simply sending individual qubits across such large distances is not feasible. Often qubits for use within communication protocols are realised physically as photons that are sent along optical fibres. However, the probability of a photon being absorbed increases exponentially as the length of the fibre it is sent along increases. Further, if a photon is successfully transmitted, the fidelity of the shared entangled state decreases exponentially as the distance increases.

Quantum teleportation [21] is used in quantum communication to transfer the information encoded within the state of single qubit held by one party to a different party at another location. In teleportation the qubit itself is not sent between the parties and a copy cannot be produced and transmitted due to the No-Cloning Theorem [22, 23]. Instead, teleportation relies on the two parties sharing an entangled resource state in the form of a Bell pair. The first party measures the qubits they hold and sends information regarding the outcome of this measurement via a classical communication channel, which is used by the second party to perform a corrective operation to their qubit that will subsequently be in the desired state. This demonstrates the need for shared entangled resource states within quantum communication protocols.

Quantum repeaters [24, 25] are used to generate entangled pairs over large distances. The full distance is split into shorter sections where entangled pairs are established. This entanglement can be 'swapped' [26] in an extension of quantum teleportation to combine two entangled pairs across a greater distance. Purification protocols [27, 28] are used on multiple copies of noisy pairs established via entanglement swapping to probabilistically increase the fidelity of the shared state. Several repeater designs have subsequently been put forward including schemes that perform entanglement generation and swapping using atomic ensembles and

single-photon detectors [29], or two-photon detectors [30, 31]. Other proposals use multiplexing [32], which offers multiple opportunities to establish entanglement connections, and several schemes make use of spin states within Nitrogen-Vacancy (NV) centres [33–35]. Graph states can be used as a resource within quantum repeaters, including in the repeater designs of [36, 37].

Another method to address errors in quantum states due to noise or decoherence, where information is 'leaked' to the environment, is through Quantum Error Correction (QEC) [38, 39]. QEC encodes a quantum state within a larger entangled state that can be measured without disturbing the information to determine and correct any errors. The stabilizer formalism was first introduced by Gottesman [40] to provide a convenient and concise mathematical description of certain QEC codes. However, the stabilizer formalism can also be applied to graph states, which is the focus of this work.

1.2 Thesis Outline

Chapter 2 covers the mathematical framework of quantum mechanics, with an emphasis on the class of entangled states known as graph states [17] and their concise description using the stabilizer formalism [40]. The subsequent chapters address different scenarios where graph states and the stabilizer formalism are utilised. These chapters are independent of one another and each should be comprehensible with the aid of the background material of Chapter 2; the presented arrangement simply corresponds to the order in which the work was completed.

In Chapter 3 we analyse the entanglement structure of graph states by calculating the purity of reduced states of graph states entirely within the stabilizer formalism, using only the stabilizer generators for a given state. We use these results to evaluate the Concentratable Entanglement [41] for several graph state examples, since this is an entanglement measure defined in terms of reduced state purities.

Chapter 4 presents an adapted version of Measurement Based Quantum Computation (MBQC) [15, 16], in which a graph state with specified additional operations is used as an entangled resource state to perform a two-qubit unitary. The stabilizer formalism and rules for graph state measurement are applied to reduce the number of qubits required to implement the protocol.

In Chapter 5 we study how spin-photon interactions in a cavity [42, 43] can be used to generate stabilizer states probabilistically even when the phase shift induced by the interaction is small. The scheme acts as a heralded Bell state source and can be used to produce larger photonic states that are locally equivalent to graph states. We note that only certain aspects of the interaction and subsequent measurement can be tracked using the stabilizer formalism.

Finally, we summarise the work, discussing how the stabilizer formalism was utilised in the three scenarios and we consider future extensions of each project.

Chapter 2

Mathematical Background

2.1 Postulates of Quantum Mechanics

Quantum Mechanics requires rules, or postulates, in order to mathematically formulate descriptions of physical systems [44].

States: A state $|\psi\rangle$ of a physical system is a ray within a Hilbert space $\mathcal{H}$ over the complex numbers $\mathbb{C}$.

A ray is the set of all vectors describing the same state. Vectors that differ by a phase factor $\lambda \in \mathbb{C}, \lambda \neq 0$ are elements of the same ray.

A qubit is a two-level system, with two-dimensional Hilbert space $\mathcal{H} = \mathbb{C}^2$. A general qubit state is written in the form

$$|\psi\rangle = \alpha\,|0\rangle + \beta\,|1\rangle\,, \tag{2.1}$$

where $\alpha, \beta \in \mathbb{C}$, $|\alpha|^2 + |\beta|^2 = 1$ to normalise the state, and the states $|0\rangle$ and $|1\rangle$ form an orthonormal basis known as the computational basis.

Observables: A physical quantity of a system corresponds to an observable, which is a self-adjoint or Hermitian operator A in Hilbert space.

An operator is Hermitian if $A = A^\dagger$. A Hermitian operator has a complete set of eigenstates that form an orthonormal basis for $\mathcal{H}$ and real eigenvalues, which are the possible values of the physical quantity associated with the observable. An eigenvalue is degenerate if it is associated with multiple eigenstates. Each eigenstate $|\phi_{jk}\rangle$ of A is related to its corresponding eigenvalue $a_j \in \mathbb{R}$ by

$$A\,|\phi_{jk}\rangle = a_j\,|\phi_{jk}\rangle\,. \tag{2.2}$$

Furthermore, each eigenvalue a_j is associated with a projection operator $\mathcal{P}_j$ on a d-dimensional subspace spanned by the eigenstates $|\phi_{jk}\rangle$,

$$\mathcal{P}_j = \sum_{k=1}^{d} |\phi_{jk}\rangle \langle\phi_{jk}| , \tag{2.3}$$

where d is the multiplicity of the eigenvalue. The spectral decomposition of the operator A is

$$A = \sum_j a_j \mathcal{P}_j. \tag{2.4}$$

Measurements: i. When an observable is measured the possible outcomes are the eigenvalues. The probability of obtaining outcome a_j is

$$p(a_j) = \langle\psi|\mathcal{P}_j|\psi\rangle . \tag{2.5}$$

The expectation value of the observable A for a system in the state $|\psi\rangle$ is

$$\langle A\rangle = \langle\psi|A|\psi\rangle = \sum_j a_j p(a_j). \tag{2.6}$$

When measuring a single qubit, the possible outcomes are often labelled as 0 and 1 according to the index and listed order of the eigenstates of the measured observable, rather than the corresponding eigenvalue. This assigns the eigenvalues a bit value.

ii. Following a measurement with outcome a_j, the state of the system is projected onto the normalised state

$$|\psi\rangle \to \frac{\mathcal{P}_j |\psi\rangle}{\sqrt{\langle\psi|\mathcal{P}_j|\psi\rangle}}. \tag{2.7}$$

Time Evolution: The time evolution of a closed quantum system is given by a unitary transformation, which is defined in terms of the Hamiltonian H of the system

$$U(t, t_0) = e^{-iH(t-t_0)/\hbar}. \tag{2.8}$$

An operator is unitary if $UU^\dagger = U^\dagger U = \mathbb{I}$. A state $|\psi(t_0)\rangle$ at an initial time t_0 is transformed by the unitary operator $U(t, t_0)$ to the state $|\psi(t)\rangle$ at time t;

$$|\psi(t)\rangle = U(t, t_0) |\psi(t_0)\rangle . \tag{2.9}$$

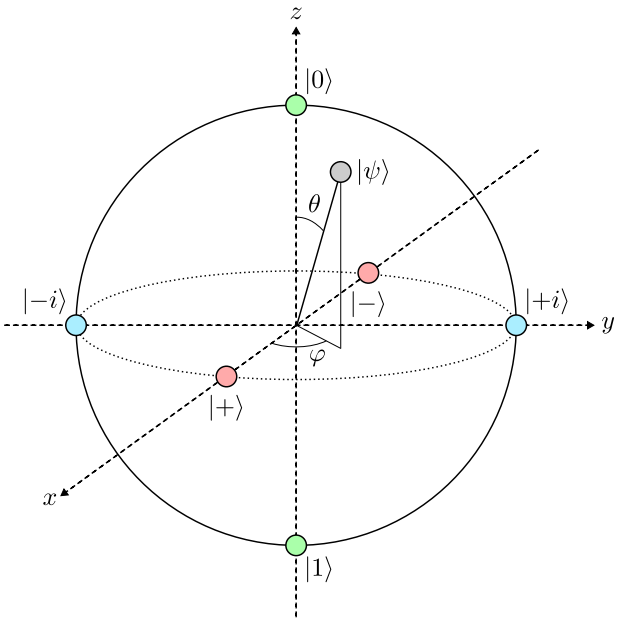

Figure 2.1: The Bloch Sphere showing a general single-qubit state $|\psi\rangle$ and the eigenstates of the Pauli operators.

2.2 Quantum States

2.2.1 Single-qubit states

One way to parameterise a single-qubit state satisfying the conditions of Eq. (2.1) is

$$|\psi\rangle = \cos(\theta/2)\,|0\rangle + e^{i\varphi}\sin(\theta/2)\,|1\rangle\,, \tag{2.10}$$

where $0 \leq \theta \leq \pi$ and $0 \leq \varphi < 2\pi$. A state corresponds to a point on the unit sphere in $\mathbb{R}^3$ by using θ and φ as the parameters for spherical coordinates where

$$\begin{aligned} x &= \sin(\theta)\cos(\varphi), \\ y &= \sin(\theta)\sin(\varphi), \\ z &= \cos(\theta). \end{aligned} \tag{2.11}$$

This representation of states is known as the Bloch sphere, shown in Fig. 2.1.

The Pauli matrices are Hermitian, traceless and unitary 2×2 matrices

$$X = \begin{pmatrix} 0 & 1 \\ 1 & 0 \end{pmatrix}, \quad Y = \begin{pmatrix} 0 & -i \\ i & 0 \end{pmatrix}, \quad Z = \begin{pmatrix} 1 & 0 \\ 0 & -1 \end{pmatrix}. \tag{2.12}$$

X acts as a bit flip operation and Z as a phase flip operation. Occasionally the identity matrix

$$\mathbb{I} = \begin{pmatrix} 1 & 0 \\ 0 & 1 \end{pmatrix} \tag{2.13}$$

is included in the set of Pauli matrices, as the four form a basis for 2×2 Hermitian matrices. Each Pauli matrix has eigenvalues ± 1 and the eigenstates for each operator are

$$\begin{aligned} X: \quad |+\rangle &= \frac{|0\rangle + |1\rangle}{\sqrt{2}}, \quad |-\rangle = \frac{|0\rangle - |1\rangle}{\sqrt{2}}, \\ Y: \quad |+i\rangle &= \frac{|0\rangle + i\,|1\rangle}{\sqrt{2}}, \quad |-i\rangle = \frac{|0\rangle - i\,|1\rangle}{\sqrt{2}}, \\ Z: \quad |0\rangle &, \quad |1\rangle . \end{aligned} \tag{2.14}$$

Note that the Z eigenstates form the computational basis.

The Bloch sphere and Pauli matrices come hand-in-hand, as the eigenstates of each Pauli matrix correspond to the points on the Bloch sphere that intersect the x, y and z axes, shown in Fig. 2.1. Further, when exponentiated, the Pauli matrices are generators of single-qubit rotations around the corresponding Cartesian axis of the Bloch sphere by an angle θ,

$$\begin{aligned} U_X(\theta) = e^{-i\theta X/2} &= \begin{pmatrix} \cos(\theta/2) & -i\sin(\theta/2) \\ -i\sin(\theta/2) & \cos(\theta/2) \end{pmatrix}, \\ U_Y(\theta) = e^{-i\theta Y/2} &= \begin{pmatrix} \cos(\theta/2) & -\sin(\theta/2) \\ \sin(\theta/2) & \cos(\theta/2) \end{pmatrix}, \\ U_Z(\theta) = e^{-i\theta Z/2} &= \begin{pmatrix} e^{-i\theta/2} & 0 \\ 0 & e^{i\theta/2} \end{pmatrix}. \end{aligned} \tag{2.15}$$

2.2.2 Density Matrices

The quantum state $|\psi\rangle$ can also be associated with a density operator ρ, which can be defined as

$$\rho = |\psi\rangle \langle\psi| . \tag{2.16}$$

However, there are cases where the state of a system may not be known and cannot be written as a vector due to incomplete information, for example due to uncertainty in the state preparation procedure or when describing a subsystem of a larger system. Here, a density operator is used to describe the system as a probabilistic mixture of states

$$\rho = \sum_i p_i \, |\psi_i\rangle \langle\psi_i| , \tag{2.17}$$

where p_i is the probability that the system is prepared in the state $|\psi_i\rangle$. The decomposition in Eq. (2.17) is not unique. Such a state is known as a mixed state. For a bipartite system with density operator ρ made up of two subsystems A and B, the density operator for the reduced state of one subsystem is found by tracing out the other subsystem, i.e. $\rho_A = \mathrm{Tr}_B \rho$.

Example. A state of two qubits is described by the density operator

$$\rho = \frac{1}{7} |00\rangle_{AB}\langle 00| + \frac{3}{7} |01\rangle_{AB}\langle 01| + \frac{1}{7} |10\rangle_{AB}\langle 10| + \frac{2}{7} |11\rangle_{AB}\langle 11| . \tag{2.18}$$

The system is made up of two subsystems A and B, which consist of the first qubit and second qubit respectively. The density matrix for the reduced state of qubit 1 is found by tracing out qubit 2,

$$\rho_A = \mathrm{Tr}_B \rho = \frac{4}{7} |0\rangle_A\langle 0| + \frac{3}{7} |1\rangle_A\langle 1| . \tag{2.19}$$

Similarly, the density matrix for the reduced state of qubit 2 is found by tracing out qubit 1,

$$\rho_B = \mathrm{Tr}_A \rho = \frac{2}{7} |0\rangle_B\langle 0| + \frac{5}{7} |1\rangle_B\langle 1| . \tag{2.20}$$

The purity of a quantum state with density matrix ρ is $\mathrm{Tr}\rho^2$. A state is pure if $\mathrm{Tr}\rho^2 = 1$. Otherwise a state is a mixed state where the purity is bound below by $1/d$, where d is the dimension of the Hilbert space of the state.

The von Neumann entropy for a quantum state with density matrix ρ is

$$S(\rho) = -\mathrm{Tr}(\rho \ln \rho). \tag{2.21}$$

This is easily calculated for a density matrix ρ written in the diagonal form of Eq. (2.17) where it reduces to the classical entropy

$$S = -\sum_i p_i \ln p_i. \tag{2.22}$$

The von Neumann entropy provides a measure of the amount of missing information that would be required to make ρ a pure state. The measure can also be applied to reduced states.

2.3 The Stabilizer Formalism

A quantum system may consist of n qubits, with a Hilbert space given by the tensor product of the Hilbert spaces of each individual qubit, $\mathcal{H} = (\mathbb{C}^2)^{\otimes n}$. Writing the state of n qubits as a linear combination of computational basis states requires up

to 2^n terms. This can lead to lengthy calculations when considering operations on the state. Instead, certain quantum states can be described fully by n terms by using the stabilizer formalism, first introduced by Gottesman to describe Quantum Error Correction (QEC) codes [40].

An n qubit state $|\psi\rangle$ is a stabilizer state if it can be associated with a stabilizer group $\mathfrak{S}_\psi$ with elements $S \in \mathfrak{S}_\psi$ that satisfy

$$S\,|\psi\rangle = |\psi\rangle\,. \tag{2.23}$$

Each stabilizer element S is also an element of the n-qubit Pauli group. The Pauli group for a single qubit is

$$\mathcal{G}_1 = \{\pm 1, \pm i\} \times \{\mathbb{I}, X, Y, Z\}, \tag{2.24}$$

which is the group generated by the Pauli matrices. For n qubits, the Pauli group is $\mathcal{G}_n = \mathcal{G}_1^{\otimes n}$. The stabilizer forms an Abelian group under multiplication and the product of any two elements is itself an element of the stabilizer.

An Abelian group $(G, *)$ is a set G and a binary operation $*$ on G satisfying the group axioms and an additional condition of commutativity:

- The group is closed under the operation $*$, i.e. $a * b \in G$ for all $a, b \in G$.
- The operation $*$ is associative, i.e. $a * (b * c) = (a * b) * c$ for any $a, b, c \in G$.
- An identity element $e \in G$ exists and satisfies $e * a = a = a * e$ for all $a \in G$.
- There exists an inverse element $a^{-1} \in G$ for each $a \in G$ such that $a * a^{-1} = e = a^{-1} * a$.
- The operation $*$ is commutative, i.e. $a * b = b * a$ for all $a, b \in G$.

The stabilizer $\mathfrak{S}_\psi$ for an n qubit state contains 2^n elements, which does not appear to simplify the description of an n qubit state. However, the stabilizer and therefore the associated quantum state can be fully specified by n terms known as stabilizer generators. These n generators together with the group operation of multiplication can be used to recover the full stabilizer.

When an operator U is applied to the stabilizer state $|\psi\rangle$, the elements of the stabilizer $S \in \mathfrak{S}_\psi$ are updated according to

$$S \to USU^\dagger. \tag{2.25}$$

The updated stabilizer element stabilizes the state where the operator U is applied since

$$[USU^\dagger]U\,|\psi\rangle = US\,|\psi\rangle = U\,|\psi\rangle\,, \tag{2.26}$$

using Eq. (2.23). Only the stabilizer generators for the state $|\psi\rangle$ need to be updated when U is applied, as they can be used to generate the full stabilizer for $U|\psi\rangle$. In order for the updated state to be a stabilizer state in itself, the operator U must be an element of the Clifford group. The Clifford group $\mathcal{C}_n$ contains all unitary operators that result in an element of the Pauli group when applied to an element of the Pauli group. Every element $U \in \mathcal{C}_n$ satisfies

$$UP_iU^\dagger = P_j, \tag{2.27}$$

where $P_i, P_j \in \mathcal{G}_n$. The Clifford group is generated by the Hadamard, phase and Controlled-Z (CZ) gates. The Hadamard gate, H, transforms the computational basis states to the X eigenstates and vice-versa,

$$H = \frac{1}{\sqrt{2}}\begin{pmatrix} 1 & 1 \\ 1 & -1 \end{pmatrix}. \tag{2.28}$$

The phase gate, Φ, is a rotation by π about the z axis,

$$\Phi = \begin{pmatrix} 1 & 0 \\ 0 & i \end{pmatrix}. \tag{2.29}$$

The CZ gate is a two-qubit gate and applies a Pauli Z operation to the target qubit only when the control qubit is in the state $|1\rangle$,

$$\mathrm{CZ} = \begin{pmatrix} 1 & 0 & 0 & 0 \\ 0 & 1 & 0 & 0 \\ 0 & 0 & 1 & 0 \\ 0 & 0 & 0 & -1 \end{pmatrix}. \tag{2.30}$$

An important theoretical result relating to operations and measurements that can be managed and described by the stabilizer formalism is the Gottesman-Knill Theorem [45], which is itself derived from and proved by the construction of the formalism and Clifford group.

Gottesman-Knill Theorem. A quantum computer acting on a stabilizer state applying only measurements of Pauli group operators and Clifford operations that may depend on previous measurement outcomes can be perfectly simulated in polynomial time on a probabilistic classical computer.

The stabilizer formalism allows for quantum computations involving stabilizer states, Clifford operations and Pauli measurements to be efficiently tracked. A stabilizer state of n qubits is specified by $n(2n+1)$ classical bits. Each of the n generators requires 2 bits to determine the n Pauli matrices (including the identity) and a further bit for the phase ± 1. The effect of a Clifford operation U is tracked by updating each generator using Eq. (2.25), which results in another stabilizer

state. Similarly, a quantum computation involving a Pauli measurement of a stabilizer state can be treated using only the stabilizer generators by manipulating the generators for the remaining state to commute with the Pauli operator. This is discussed in more detail in Section 2.5.

An n qubit state requires n stabilizer generators to be fully described, as each generator halves the dimension of the remaining subspace until only one possible state remains. However stating fewer than n stabilizer generators defines a subspace of the n qubit Hilbert space with dimension larger than 1. The states that span this subspace all satisfy Eq. (2.23) for each of the stated stabilizer generators. In QEC — the original proposed application for the stabilizer formalism, a state that requires protection from errors can be encoded within the states that span such a subspace. Since Eq. (2.23) is satisfied, measurement of any of the stabilizer generators should result in the outcome $+1$. However if an error occurs, measurement of certain generators can result in the outcome -1. The pattern of the minus signs within the measurement outcomes, known as the error syndrome, identifies the error that has occurred, which can subsequently be corrected. To demonstrate a stabilizer code, consider the simple example of a three qubit code to detect a single bit flip error [46].

Example. A single qubit state is encoded into a state of three physical qubits,

$$\alpha\,|0\rangle + \beta\,|1\rangle \xrightarrow{encode} \alpha\,|000\rangle + \beta\,|111\rangle\,. \tag{2.31}$$

The stabilizer generators for the two-dimensional subspace spanned by the states $|000\rangle$ and $|111\rangle$ are Z_1Z_2 and Z_2Z_3. By measuring these generators and recording the outcomes, the qubit that has been affected by a bit flip error can be identified.

Error	Syndrome
None	$+1,+1$
X_1	$-1,+1$
X_2	$-1,-1$
X_3	$+1,-1$

2.4 Graph States

One class of quantum states to which the stabilizer formalism can be applied is graph states [17]. These are associated with mathematical graphs and have a wide range of applications, including QEC [40, 47, 48] and the One-Way Quantum Computer [15, 16].

A graph $G = (V, E)$ consists of a set of vertices V and a set of edges E that connect pairs of vertices. When used to visualise quantum states, each vertex represents a qubit in the state $|+\rangle$, and edges denote CZ operations between pairs

of qubits. The case where a graph state forms a regular lattice in one or more dimensions is known as a cluster state.

The neighbourhood $n(a)$ of a vertex $a \in V$ is the set of vertices connected to the selected vertex by a single edge. In a graph state this identifies the qubits that jointly undergo a CZ operation with qubit a. For a graph state consisting of n qubits, an $n \times n$ adjacency matrix A can also be used to define the neighbourhoods within a graph, with entries $A_{ij} = 0$ where vertices i and j are not connected and $A_{ij} = 1$ where i and j are joined by an edge.

To describe graph states within the stabilizer formalism, each vertex a within the graph can be associated with a stabilizer generator of the form

$$S_a = X_a \prod_{b \in n(a)} Z_b. \tag{2.32}$$

Example. Fig. 2.2 shows a graph with four vertices that represents a quantum state of four qubits. By observation of the edges within the graph, the neighbourhood $n(a)$ for each vertex $a \in V$ is found and the qubits that jointly undergo CZ operations are determined.

Qubit a	Neighbourhood $n(a)$
1	$\{2\}$
2	$\{1, 3, 4\}$
3	$\{2, 4\}$
4	$\{2, 3\}$

The sets of neighbouring qubits for each qubit within the graph are used in Eq. (2.32) to find the stabilizer generators of the four qubit state:

$$\begin{aligned} S_1 &= X_1 Z_2 \\ S_2 &= Z_1 X_2 Z_3 Z_4 \\ S_3 &= \quad Z_2 X_3 Z_4 \\ S_4 &= \quad Z_2 Z_3 X_4. \end{aligned} \tag{2.33}$$

2.5 Pauli Measurements

Performing a measurement of a Pauli operator on a single qubit of a graph state can be considered within the stabilizer formalism. As an immediate consequence of such a measurement, the measured qubit is removed from the graph state.

The simplest measurement to describe on a graph state is that of the Pauli Z operator on a single qubit. Depending on the measurement outcome with possible

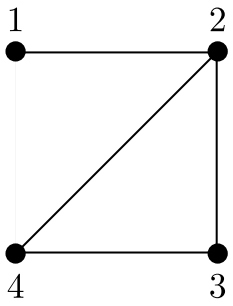

Figure 2.2: A four qubit graph state.

values $+1$ or -1, the individual qubit is in one of the two eigenstates of the Z operator, $|0\rangle$ or $|1\rangle$ with stabilizer generator Z or $-Z$ respectively.

Though the measured qubit is disconnected from the graph state, it still affects the remaining state due to its entanglement prior to the measurement. When qubit $a \in V$ is measured the graph becomes $G' = G - \{a\}$ where all edges to vertex a are removed. The state of the remaining qubits is $U|G - \{a\}\rangle$ where U is a unitary operator determined by the measurement outcome. For the outcomes ± 1 the unitaries are [17]

$$U_+ = \mathbb{I} \quad \text{and} \quad U_- = \prod_{b \in n(a)} Z_b. \tag{2.34}$$

In the stabilizer formalism a stabilizer generator S'_b for each remaining vertex $b \in V'$ is determined using Eq. (2.32). Then the unitary operator corresponding to the outcome is applied to each generator as $US'_bU^\dagger$ to give the generators for the state $U|G - \{a\}\rangle$.

An alternative method, which will be used more prominently in this work, is to take the original set of stabilizer generators for $|G\rangle$ and set the stabilizer generator for the measured qubit to $\pm Z_a$ depending on the measurement outcome. The generators for qubits that were not within the neighbourhood of qubit a remain unchanged. However the generators for qubits within the neighbourhood of the measured qubit, which contain the term Z_a, are multiplied by the new generator $\pm Z_a$, allowed by the group structure of the new stabilizer. This enables the new stabilizer generators to be found without explicitly drawing the graph representing the quantum state.

Similar rules and unitary operators are given [17, 49] for measurements in the X and Y directions, which are considered to be more complex. An X direction measurement results in a graph and unitary operators that depend on a selected qubit b_0 in the neighbourhood of a. A Y measurement of qubit a inverts the subgraph containing the qubits in $n(a)$, which removes qubit a. Within the stabilizer formalism the stabilizer generators for the remaining state following an X

or Y measurement are found by setting the generator for the measured qubit to correspond to the appropriate eigenstate of the X or Y Pauli operator and using the group structure of the stabilizer to find the generator associated with each remaining qubit. Pauli X and Y measurements are explained in more detail and applied in Chapter 4.

2.6 Quantum Entanglement

Entanglement [13, 14] is a phenomenon where spatially separated systems exhibit correlated behaviour and is not present within the classical description of the physical world. It is an essential resource for quantum communication in protocols such as teleportation [21], quantum computing and Quantum Key Distribution (QKD) [10, 11]. Entanglement measures can be used to analyse the structure of entanglement within a quantum state and determine states that can be used within quantum information transmission.

Entanglement measures must satisfy two standard postulates [50]:

1. Any measure must be monotonic.

   The value of the measure cannot increase under Local Operations and Classical Communication (LOCC), where results from operations on one part of a system would be transmitted and used to determine further operations on another subsystem.

2. Any measure must be zero for separable states.

   A separable state can be written as the product of the individual states of any subsystems.

Entanglement across the two subsystems within a bipartite quantum state is well understood. A widely used quantitative measure is entanglement of formation [51], which for pure states coincides with the von Neumann entropy of the reduced state of either subsystem [52, 53], known as the entropy of entanglement. The definition of entanglement of formation can be extended to mixed states by considering ensembles of pure states.

Concurrence is an entanglement measure for a two-qubit state [54]. It is given by

$$C(\psi) = |\langle\psi|\tilde{\psi}\rangle|, \tag{2.35}$$

where $|\tilde{\psi}\rangle = Y|\psi^*\rangle$ is the spin flip state with $|\psi^*\rangle$ denoting the complex conjugate of the state $|\psi\rangle$ [55]. On the Bloch sphere, complex conjugation is equivalent to reflection in the x-z plane and applying the Pauli Y operator is a rotation by π about the y-axis.

Though it would appear that concurrence provides a new measure of the entanglement of two qubits, it is related to the entanglement of formation by a monotonic function [54]. Concurrence can be generalised from two qubit states to apply to pure states with bipartite entanglement [56].

For two-qubit states, there is only one type of entanglement, seen in the maximally entangled Bell states:

$$\begin{aligned} |\Phi^{\pm}\rangle &= \frac{|00\rangle \pm |11\rangle}{\sqrt{2}}, \\ |\Psi^{\pm}\rangle &= \frac{|01\rangle \pm |10\rangle}{\sqrt{2}}. \end{aligned} \tag{2.36}$$

Together these states form the Bell basis, an orthonormal basis for the four dimensional Hilbert space for two qubits. Entanglement of formation can be interpreted as an upper limit on how many Bell pairs can be distilled from a state, or equivalently, how many were consumed in forming the state. Bell states are stabilizer states with stabilizer generators:

State	S_1	S_2
$\|\Phi^+\rangle$:	X_1X_2	Z_1Z_2
$\|\Phi^-\rangle$:	$-X_1X_2$	Z_1Z_2
$\|\Psi^+\rangle$:	X_1X_2	$-Z_1Z_2$
$\|\Psi^-\rangle$:	$-X_1X_2$	$-Z_1Z_2$.

(2.37)

Though the Bell pairs are not graph states, since their stabilizer generators are not of the form of Eq. (2.32), they are Local Unitary (LU) equivalent. The Bell states can be transformed to the two-qubit graph state by applying specific Clifford group operators to single qubits within each state.

Entanglement in multipartite states is more difficult to characterise and quantify, as the ways in which a state can be entangled increases with the number of parties involved. A widely cited example of different kinds of entanglement, first discussed by Dür et al. [57], is demonstrated when considering three party entanglement, as the entanglement present in a three qubit GHZ state [1] differs from that in a three qubit W state [2]. It is not possible to transform either state to the other using LOCC. Several existing multipartite measures are functions of bipartite entanglement measures [58–60], sometimes considered over multiple bipartitions of the state. Multipartite entanglement measures that are computationally simple are often favoured.

[1] $|\mathrm{GHZ}\rangle = (|000\rangle + |111\rangle)/\sqrt{2}$

[2] $|\mathrm{W}\rangle = (|100\rangle + |010\rangle + |001\rangle)/\sqrt{3}$

The Greenberger-Horne-Zellinger (GHZ) state [61, 62] is of further interest as it is a stabilizer state. The GHZ state for n qubits is

$$|\mathrm{GHZ}\rangle = \frac{|0\rangle^{\otimes n} + |1\rangle^{\otimes n}}{\sqrt{2}}, \tag{2.38}$$

and has stabilizer generators [63]

$$\begin{aligned} S_1 &= X_1 X_2 X_3 \cdots X_{n-1} X_n \\ S_2 &= Z_1\, Z_2 \\ S_3 &= \quad Z_2\, Z_3 \\ &\vdots \\ S_n &= \qquad\qquad Z_{n-1} Z_n. \end{aligned} \tag{2.39}$$

The GHZ state is LU equivalent to the star graph state, in which a central qubit jointly undergoes a CZ operation with each outer qubit. To transform between the star graph and GHZ state a Hadamard operation is applied to each of the outer qubits.

Chapter 3

Concentratable Entanglement of Graph States

The entanglement present in graph states makes them a useful resource in quantum information processing. When used for Measurement Based Quantum Computation (MBQC) [64] and the One-Way Quantum Computer [15, 16], the specific computation dictates the structure of the graph state. Conversely, the entanglement structure of a graph state determines its effectiveness in applications such as the quantum repeater [24, 36, 37], QEC codes [40, 47] and quantum secret sharing [65]. An entanglement measure is required to investigate the structure of the multipartite entanglement within a graph state.

A recently proposed multipartite entanglement measure is Concentratable Entanglement [41]. This is shown to be a valid pure state entanglement measure [41], as it satisfies the two standard postulates for entanglement measures [50] concerning monotonicity under LOCC and vanishing on separable states. Further properties of the measure are demonstrated including subadditivity and continuity. When defined for different cuts of qubits within a state, Concentratable Entanglement relates to several existing measures [54, 56, 58–60, 66, 67], making it a candidate for adoption as the universal multipartite entanglement measure of pure states. Like other measures, one approach to calculating Concentratable Entanglement is to consider bipartitions of the multipartite quantum state. The purities of the corresponding reduced density matrices are required to evaluate the Concentratable Entanglement.

The multipartite entanglement of graph states has previously been investigated in terms of Schmidt measure and Schmidt rank [17, 68], which can be challenging to compute. Concentratable Entanglement offers a new measure that can be applied to graph states. Using the stabilizer formalism, we have developed a method reliant only on the stabilizer generators for determining reduced state purities and thus Concentratable Entanglement for graph states. This allows for calculation of the

Concentratable Entanglement for examples such as single qubits in graph states, for subsets of qubits within graph states proposed for use in quantum repeaters and as a measure of the overall entanglement for any graph state.

This chapter is largely based on [69] with any mathematical background information covered within Chapter 2 omitted to avoid repetition and an update to the discussion regarding mixed states.

3.1 Concentratable Entanglement

Concentratable Entanglement [41] can be used as a measure of multipartite entanglement of a pure quantum state $|\psi\rangle$. For a state of n qubits with labels in $\mathcal{S} = \{1, \ldots, n\}$, the Concentratable Entanglement can be calculated for the full set to determine the overall entanglement, or it can be applied to any non-empty subset $s \subseteq \mathcal{S}$ to investigate the structure of the entanglement within the state. Operationally, the Concentratable Entanglement corresponds to the probability of producing Bell pairs in a SWAP test [70]. The Concentratable Entanglement of $|\psi\rangle$ can be defined in terms of SWAP test outcomes, making it possible to efficiently calculate its value using quantum computers and two copies of $|\psi\rangle$.

However, without the physical resource of a quantum computer, the definition of the Concentratable Entanglement in terms of purities still offers a method to determine the entanglement of a (subset of a) state. For a non-empty set of qubit labels $s \subseteq \mathcal{S}$, the Concentratable Entanglement is [41]

$$C_{|\psi\rangle}(s) = 1 - \frac{1}{2^{|s|}} \sum_{\alpha \in \mathcal{P}(s)} \mathrm{Tr}\rho_\alpha^2, \tag{3.1}$$

where ρ_α is the density matrix of the reduced state with qubits labelled by the set α, which is a subset of the power set $\mathcal{P}(s)$. This requires the calculation of up to 2^n purities, including the trivial case $\mathrm{Tr}\rho_\emptyset^2 = 1$.

3.2 Purities of Reduced Graph States

Calculating the purities required within the Concentratable Entanglement relies on the reduced states of different subsets of qubits. Within the stabilizer formalism, a reduced state can be described as a mixture of several pure states, each of which has its own set of stabilizer generators. We show that the number of distinct sets of stabilizer generators corresponds to the purity of the reduced state that the sets of generators collectively describe.

Consider a bipartition (A, B) of qubits within the graph G. The reduced state of the qubits in B is found by tracing out the qubits in A

$$\rho_B = \mathrm{Tr}_A(|G\rangle \langle G|). \tag{3.2}$$

This partial trace is equivalent to measuring the qubits in A and discarding the outcome. These measurements can be performed in the Z direction, where the outcomes ± 1 each occur with probability $1/2$.

Through repeated application of the Z measurement rule and unitaries given in Eq. (2.34), and considering all possible outcomes, the density operator for the reduced state of the qubits in B is

$$\rho_B = \frac{1}{2^{|A|}} \sum_{\mathbf{z} \in \mathbb{F}_2^A} U(\mathbf{z}) \, |G - A\rangle \langle G - A| \, U(\mathbf{z})^\dagger, \tag{3.3}$$

where $\mathbb{F}_2$ is the finite field of two elements $\{0, 1\}$. An element of the finite field $\mathbb{F}_2^A$ is a bitstring $\mathbf{z}$ of length $|A|$. In $\mathbb{F}_2^A$ addition and subtraction are equivalent and performed modulo 2 without carry. The local unitaries are [17]

$$U(\mathbf{z}) = \prod_{a \in A} \left(\prod_{b \in n(a) \cap B} Z_b \right)^{z_a}, \tag{3.4}$$

where $z_a = 0$ represents the outcome $+1$ and $z_a = 1$ for -1. Within the unitaries, only qubits in the neighbourhood of measured qubits which are also in B need to be considered. This is because the individual qubits in A can be measured in any order, making it possible for neighbourhood qubits to already be disconnected from the graph. Further, Z_b for $b \in A$ has no effect on the state $|G - A\rangle$, which does not contain qubits in A.

For completeness, we prove the following properties of these unitary operators that have previously been stated and applied [17], as they provide the basis for proving our own result regarding the purities of reduced states.

Lemma. (Hein-Eisert-Briegel)

1. For different measurement outcomes $\mathbf{z}$ and $\mathbf{z}'$ to give the same unitary operator, i.e. $U(\mathbf{z}) = U(\mathbf{z}')$, the bitstrings must satisfy [17]

$$U(\mathbf{z} - \mathbf{z}') = I. \tag{3.5}$$

2. If $U(\mathbf{z}) \neq U(\mathbf{z}')$ then the states $U(\mathbf{z}) \, |G - A\rangle$ and $U(\mathbf{z}') \, |G - A\rangle$ are orthogonal.

Proof. 1. Using the definition of the unitary operator in Eq. (3.4),

$$\begin{aligned} U(\mathbf{z}-\mathbf{z}') &= \prod_{a\in A}\left(\prod_{b\in n(a)\cap B} Z_b\right)^{z_a - z'_a} \\ &= \prod_{a\in A}\left(\prod_{b\in n(a)\cap B} Z_b\right)^{z_a} \prod_{a'\in A}\left(\prod_{b'\in n(a')\cap B} Z_{b'}\right)^{-z'_{a'}} \\ &= \prod_{a\in A}\left(\prod_{b\in n(a)\cap B} Z_b\right)^{z_a} \prod_{a'\in A}\left(\prod_{b'\in n(a')\cap B} Z_{b'}^{-1}\right)^{z'_{a'}} \\ &= U(\mathbf{z})U(\mathbf{z}')^\dagger. \end{aligned} \tag{3.6}$$

This is equal to the identity

$$U(\mathbf{z}-\mathbf{z}') = U(\mathbf{z})U(\mathbf{z}')^\dagger = I \tag{3.7}$$

and by right multiplying by $U(\mathbf{z}')$, this gives $U(\mathbf{z}) = U(\mathbf{z}')$.

2. If $U(\mathbf{z}) \neq U(\mathbf{z}')$ then $U(\mathbf{z})U(\mathbf{z}')^\dagger \neq I$ using the above proof. $U(\mathbf{z})U(\mathbf{z}')^\dagger$ is a product of Pauli Z operators, as shown in Eq. (3.6), which in the simplest case consists of a single operator Z_j where $j \in B$. Qubit j in the remaining graph $G' = G - A$ is associated with a stabilizer generator S'_j in the form of Eq. (2.32) that satisfies $S'_j |G'\rangle = |G'\rangle$. The inner product of the states $U(\mathbf{z})|G-A\rangle$ and $U(\mathbf{z}')|G-A\rangle$ is

$$\begin{aligned} \langle G'| U(\mathbf{z}')^\dagger U(\mathbf{z}) |G'\rangle &= \langle G'| Z_j |G'\rangle \\ &= \langle G'| Z_j S'_j |G'\rangle \\ &= \langle G'| Z_j X_j \textstyle\prod_{b\in n(j)} Z_b |G'\rangle \\ &= \langle G'| (-X_j Z_j) \textstyle\prod_{b\in n(j)} Z_b |G'\rangle \\ &= -\langle G'| (X_j \textstyle\prod_{b\in n(j)} Z_b) Z_j |G'\rangle \\ &= -\langle G'| S_j'^\dagger Z_j |G'\rangle \\ &= -\langle G'| Z_j |G'\rangle \\ &= -\langle G'| U(\mathbf{z}')^\dagger U(\mathbf{z}) |G'\rangle . \end{aligned} \tag{3.8}$$

This is satisfied only when $\langle G'| U(\mathbf{z}')^\dagger U(\mathbf{z}) |G'\rangle = 0$ so the states $U(\mathbf{z})|G-A\rangle$ and $U(\mathbf{z}')|G-A\rangle$ are orthogonal.

More generally $U(\mathbf{z})U(\mathbf{z}')^\dagger$ can be written as

$$U(\mathbf{z})U(\mathbf{z}')^\dagger = Z_j \prod_{c\in C} Z_c \tag{3.9}$$

where C is a subset of $B \setminus j$. $\prod_{c \in C} Z_c$ commutes with S'_j so replacing Z_j by the more general expression for $U(\mathbf{z})U(\mathbf{z}')^\dagger$ in Eq. (3.8), the states $U(\mathbf{z})\,|G-A\rangle$ and $U(\mathbf{z}')\,|G-A\rangle$ satisfy $\langle G-A|\,U(\mathbf{z}')^\dagger U(\mathbf{z})\,|G-A\rangle = 0$ and hence are orthogonal. □

The unitary operators $U(\mathbf{z})$ can used within the stabilizer formalism to find the reduced state of qubits in B. The set of stabilizer generators for each outcome must be considered separately. The remaining graph $G - A$ can be found by removing all edges to qubits in A and the stabilizer generator S'_b for each qubit $b \in B$ is given by Eq. (2.32). Then for each outcome, the corresponding unitary operator must be applied to each stabilizer generator according to $U(\mathbf{z})S'_bU(\mathbf{z})^\dagger$, giving a new stabilizer for each unitary operator.

An alternative method does not require calculation of the unitary operators corresponding to each measurement outcome. Instead, in the set of stabilizer generators for the original graph G, the stabilizer generator for each qubit $a \in A$ can be set to $\pm Z_a$. Then the group structure of the stabilizer can be used to determine the stabilizer generators for the remaining graph only in terms of qubits in B. This process is repeated to give a set of stabilizer generators for each measurement outcome.

The following theorem provides a link between the sets of stabilizer generators that describe a reduced state and the purity of that reduced state. This is the main component in calculating the Concentratable Entanglement.

Theorem 1. Consider a graph state bipartitioned into sets A and B. Let $k \in \mathbb{N}$ denote the number of distinct sets of stabilizer generators for the different measurement outcomes when measuring the qubits in A. The purity of the reduced state of qubits in B is then

$$\mathrm{Tr}\rho_B^2 = \frac{1}{k}. \tag{3.10}$$

Proof. When measuring the qubits in A there are $2^{|A|}$ possible outcomes. Each outcome is represented by a bitstring $\mathbf{z} \in \mathbb{F}_2^A$, which is associated with a unitary operator $U(\mathbf{z})$. Therefore there are $2^{|A|}$ unitary operators. However, these unitaries need not be unique.

For any graph state and subset A of qubits, the outcome represented by the bitstring made entirely of zeros leads to the identity operator

$$U(\mathbf{0}) = I. \tag{3.11}$$

If $U(\mathbf{0})$ is the sole identity operator, operators $U(\mathbf{z})$ and $U(\mathbf{z}')$ are equal when $\mathbf{z} - \mathbf{z}' = \mathbf{0}$ using the Hein-Eisert-Briegel Lemma. This is solved trivially by

$\mathbf{z} = \mathbf{z}'$ but has no further solutions. Therefore when one operator is the identity, all remaining unitaries take distinct values.

Consequently, for any unitary to occur more than once, there must be further operators equal to the identity. If a second operator is the identity, i.e., $U(\mathbf{w}) = I$ for some $\mathbf{w} \neq \mathbf{0}$, the remaining elements in the finite field can be matched into pairs whose difference modulo 2 is $\mathbf{w}$. Therefore there are $2^{|A|}/2 = 2^{|A|-1}$ different unitaries, each of which occurs twice.

If a third unitary is set to the identity, $U(\mathbf{v}) = I$ for $\mathbf{v} \notin \{\mathbf{0}, \mathbf{w}\}$, then it follows that a fourth unitary, $U(\mathbf{v}')$ where $\mathbf{v}' = \mathbf{v} - \mathbf{w}$, must also be the identity. Hence

$$U(\mathbf{0}) = U(\mathbf{w}) = U(\mathbf{v}) = U(\mathbf{v}') = I. \tag{3.12}$$

For any remaining $\mathbf{z} \in \mathbb{F}_2^A$, $U(\mathbf{z})$ is equal to three other unitaries, those for which the bitstring differs from $\mathbf{z}$ by $\mathbf{w}$, $\mathbf{v}$ or $\mathbf{v}'$. There are $2^{|A|}/4 = 2^{|A|-2}$ different unitary operators, each occurring 4 times.

More generally, if there are 2^j unitary operators that are the identity where $0 \leq j \leq |A|$, then there are $k = 2^{|A|-j}$ different values for the unitary operators, each of which has multiplicity 2^j.

To find the purity of the reduced state, first the density operator must be squared. Using Eq. (3.3), this gives

$$\rho_B^2 = \frac{1}{2^{2|A|}} \sum_{\mathbf{z},\mathbf{z}'} U(\mathbf{z}) \left|G'\right\rangle \left\langle G'\right| U(\mathbf{z})^\dagger U(\mathbf{z}') \left|G'\right\rangle \left\langle G'\right| U(\mathbf{z}')^\dagger, \tag{3.13}$$

where $G' = G - A$ for brevity. By the Hein-Eisert-Briegel Lemma, if $U(\mathbf{z}) \neq U(\mathbf{z}')$ then $\left\langle G'\right| U(\mathbf{z})^\dagger U(\mathbf{z}') \left|G'\right\rangle = 0$ since the states $U(\mathbf{z}) \left|G'\right\rangle$ and $U(\mathbf{z}') \left|G'\right\rangle$ are orthogonal. In the 2^j cases when $U(\mathbf{z}) = U(\mathbf{z}')$, including the case $\mathbf{z} = \mathbf{z}'$, $\left\langle G'\right| U(\mathbf{z})^\dagger U(\mathbf{z}') \left|G'\right\rangle = 1$. This leads to

$$\rho_B^2 = \frac{2^j}{2^{2|A|}} \sum_{\mathbf{z} \in \mathbb{F}_2^A} U(\mathbf{z}) \left|G'\right\rangle \left\langle G'\right| U(\mathbf{z})^\dagger = \frac{1}{k} \rho_B. \tag{3.14}$$

The trace is then taken, resulting in a purity given by

$$\mathrm{Tr}\rho_B^2 = \frac{1}{k}, \tag{3.15}$$

since $\mathrm{Tr}\rho_B = 1$.

If there are k different unitaries, this leads to k different sets of stabilizer generators to describe the graph state once the qubits in A have been removed by measurement. Each of the k unitaries is applied to give a set of generators according to $US_b'U^\dagger$ for all $b \in B$. □

For any bipartition, the purities of the reduced states ρ_A and ρ_B are related by [71]

$$\mathrm{Tr}\rho_A^2 = \mathrm{Tr}\rho_B^2, \tag{3.16}$$

due to the Schmidt decomposition theorem. When calculating purities using Theorem 1, the smaller partition from (A, B) can be traced out, reducing the number of bipartitions of an n qubit state to consider by one half.

Theorem 1 also applies when using the alternative method of finding sets of stabilizer generators without calculating the unitary operators, since this method results in the same sets of stabilizer generators.

3.3 Examples

The result of Theorem 1 can be applied within the stabilizer formalism to calculate the Concentratable Entanglement for cuts of qubits of graph states with different designs and applications. We will consider several examples here.

1. Single qubits. The Concentratable Entanglement for a set containing a single qubit a in an n qubit graph state $|G\rangle$ is

$$C_{|G\rangle}(\{a\}) = \frac{1}{4}. \tag{3.17}$$

To show this, consider any connected graph state of n qubits. To find the Concentratable Entanglement for a set s containing a single qubit, the purity of the reduced state of the single qubit must be calculated. The reduced state can be found by tracing out the other $n-1$ qubits and considering all 2^{n-1} possible measurement outcomes. However this can be simplified by instead using Eq. (3.16) and only tracing out the qubit of interest. When bipartioning the set $\mathcal{S} = \{1, \ldots, n\}$ of all qubit labels, the set $A = \{a\}$ contains a single qubit and $B = \mathcal{S} \setminus \{a\}$ contains the remaining $n-1$ qubits.

The stabilizer generators for the graph take three forms. Firstly, qubit a has the stabilizer generator

$$S_a = X_a \prod_{b \in n(a)} Z_b. \tag{3.18}$$

Second, the stabilizer generator for each qubit $b \in n(a)$ is

$$S_b = Z_a X_b \prod_{k \in \tilde{n}(b)} Z_k, \tag{3.19}$$

where $\tilde{n}(b) = n(b) \setminus \{a\}$. Finally, qubits $c \in B \setminus n(a)$ have stabilizer generators of the form

$$S_c = X_c \prod_{m \in n(c)} Z_m, \tag{3.20}$$

where $n(c)$ cannot contain qubit a.

By tracing out qubit a, its stabilizer generator must be updated to $\pm Z_a$. In both cases generators in the form of S_c remain valid. However each S_b must be multiplied by $\pm Z_a$ so the new generator contains only Pauli operators acting on qubits in B. The possible sets of stabilizer generators are

$$\begin{array}{cc} Z_a & -Z_a \\ S'_b = X_b \prod_{k\in\tilde{n}(b)} Z_k & S'_b = -X_b \prod_{k\in\tilde{n}(b)} Z_k \\ S'_c = X_c \prod_{m\in n(c)} Z_m & S'_c = \quad X_c \prod_{m\in n(c)} Z_m, \end{array}$$

where there is a stabilizer generator in both sets for each $b \in n(a)$ and each $c \in B \setminus n(a)$. The stabilizer generators for qubits in the neighbourhood of qubit a acquire a minus sign when the measurement outcome is -1.

There are two possible sets of stabilizer generators to describe the reduced states of qubits in B. Applying Theorem 1 and Eq. (3.16), the purity is

$$\mathrm{Tr}\rho_B^2 = \frac{1}{2} = \mathrm{Tr}\rho_a^2. \tag{3.21}$$

Therefore the Concentratable Entanglement for a single qubit within any connected graph state, where $s = \{a\}$, is

$$C_{|G\rangle}(\{a\}) = 1 - \frac{1}{2}(1 + \mathrm{Tr}\rho_a^2) = \frac{1}{4}. \tag{3.22}$$

2. A six qubit graph. Fig. 3.1 shows a graph state with qubit labels $\mathcal{S} = \{1, \ldots, 6\}$. This is graph No. 13 according to the standard numbering of graph state local unitary (LU) equivalence classes [17, 72, 73]. The graph is described by stabilizer generators

$$\begin{array}{ll} S_1 = X_1 Z_2 & \\ S_2 = Z_1 X_2 Z_3 & \\ S_3 = \quad Z_2 X_3 Z_4 \quad Z_6 & \\ S_4 = \quad\quad Z_3 X_4 Z_5 & \\ S_5 = \quad\quad\quad Z_4 X_5 & \\ S_6 = \quad\quad Z_3 \quad\quad X_6. & \end{array} \tag{3.23}$$

To find the purity of the reduced state of qubits 1, 2, 3 and 5, qubits 4 and 6 must be traced out. The stabilizer generators for qubits 4 and 6 are set to $\pm Z_4$ and $\pm Z_6$ to account for all possible measurement outcomes, where qubits 4 and 6

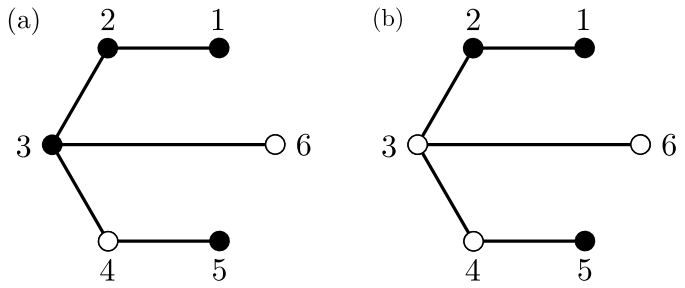

Figure 3.1: A six qubit graph state. The qubit labels can be bipartitioned, with qubits in set A represented by hollow vertices and qubits in set B by filled vertices. (a) $A = \{4, 6\}$, $B = \{1, 2, 3, 5\}$. (b) $A = \{3, 4, 6\}$, $B = \{1, 2, 5\}$.

collapse into the eigenstates of the Z operator. This results in the following sets of stabilizer generators to describe the remaining state

$$\begin{array}{cc}
\{Z_4, Z_6\} & \{Z_4, -Z_6\} \\
S_1' = X_1 Z_2 & S_1' = X_1 Z_2 \\
S_2' = Z_1 X_2 Z_3 & S_2' = Z_1 X_2 Z_3 \\
S_3' = \quad Z_2 X_3 & S_3' = \quad -Z_2 X_3 \\
S_5' = \qquad X_5 & S_5' = \qquad X_5 \\
\{-Z_4, Z_6\} & \{-Z_4, -Z_6\} \\
S_1' = X_1 Z_2 & S_1' = X_1 Z_2 \\
S_2' = Z_1 X_2 Z_3 & S_2' = Z_1 X_2 Z_3 \\
S_3' = \quad -Z_2 X_3 & S_3' = \quad Z_2 X_3 \\
S_5' = \qquad -X_5 & S_5' = \qquad -X_5.
\end{array}$$

There are four distinct sets of stabilizer generators and therefore by Theorem 1 the purity of the reduced state of qubits 1, 2, 3 and 5 is

$$\mathrm{Tr}\rho_{1235}^2 = \frac{1}{4}. \tag{3.24}$$

Instead, if qubits 3, 4 and 6 are traced out, the stabilizer generators for each of these qubits must be changed to consider all possible outcomes. Since the stabilizer generators where qubits 4 and 6 are traced out have already been calculated, only the stabilizer generator for qubit 3 needs to be updated. The stabilizer generator for qubit 3 is set to $\pm Z_3$ within each set. Therefore the sets of stabilizer generators

for the remaining qubits are

$$\{Z_3, Z_4, Z_6\},\ \{Z_3, Z_4, -Z_6\} \qquad \{-Z_3, Z_4, Z_6\},\ \{-Z_3, Z_4, -Z_6\}$$

$$\begin{aligned} S_1'' &= X_1 Z_2 \\ S_2'' &= Z_1 X_2 \\ S_5'' &= \quad X_5 \end{aligned} \qquad \begin{aligned} S_1'' &= \quad X_1 Z_2 \\ S_2'' &= -Z_1 X_2 \\ S_5'' &= \quad X_5 \end{aligned}$$

$$\{Z_3, -Z_4, Z_6\},\ \{Z_3, -Z_4, -Z_6\} \qquad \{-Z_3, -Z_4, Z_6\},\ \{-Z_3, -Z_4, -Z_6\}$$

$$\begin{aligned} S_1'' &= X_1 Z_2 \\ S_2'' &= Z_1 X_2 \\ S_5'' &= -X_5 \end{aligned} \qquad \begin{aligned} S_1'' &= \quad X_1 Z_2 \\ S_2'' &= -Z_1 X_2 \\ S_5'' &= -X_5. \end{aligned}$$

Though there are eight possible measurement outcomes, this results in only four distinct sets of stabilizer generators. Therefore by Theorem 1 the purity of the reduced state of qubits 1, 2 and 5 is

$$\mathrm{Tr}\rho_{125}^2 = \frac{1}{4}. \tag{3.25}$$

This is also the purity of the state ρ_{346} due to Eq. (3.16) and of the states ρ_{145} and ρ_{236} because of the symmetry of the graph in Fig. 3.1.

This method can be used to find the purities of all possible reduced states of the graph state. For the six bipartitions where the smaller set contains a single qubit, the purity is 1/2 from Example 1. When the smaller set in the bipartition contains two qubits, a purity of 1/4 occurs twelve times and a purity of 1/2 occurs three times. For the ten bipartitions where each set has three elements, the purity is 1/8 in four cases, 1/4 in four cases and 1/2 in two cases. These values can be used to calculate the Concentratable Entanglement of any subset of qubits and the overall Concentratable Entanglement of the graph state:

$$\begin{aligned} C_{|G_{13}\rangle}(\mathcal{S}) &= 1 - \frac{1}{2^6}\left[1 + 6\cdot\frac{1}{2} + \left(12\cdot\frac{1}{4} + 3\cdot\frac{1}{2}\right) + \left(8\cdot\frac{1}{8} + 8\cdot\frac{1}{4} + 4\cdot\frac{1}{2}\right)\right. \\ &\qquad \left. + \left(12\cdot\frac{1}{4} + 3\cdot\frac{1}{2}\right) + 6\cdot\frac{1}{2} + 1\right] \\ &= \frac{21}{32}. \end{aligned} \tag{3.26}$$

An alternative measure of entanglement with respect to a bipartition (A, B) is the Schmidt rank, defined as [68]

$$\mathrm{SR}_B(\psi) = \log_2[\mathrm{rank}(\rho_B)]. \tag{3.27}$$

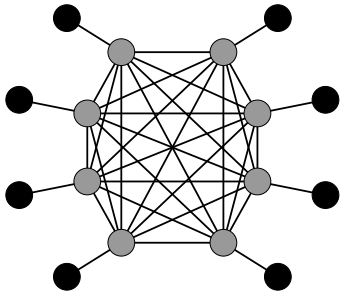

Figure 3.2: A sixteen qubit 'snowflake' state proposed for use in repeaters [37]. Grey circles represent 1st leaf qubits, each of which is connected to a 2nd leaf qubit, shown in black.

This measure is related to the purity of the reduced state of B according to [68]

$$\mathrm{SR}_B(\psi) = -\log_2[\mathrm{Tr}(\rho_B^2)]. \tag{3.28}$$

The rank index RI_m considers all bipartitions where the smaller set contains m qubits [17]. It lists the number of times the Schmidt rank m, then $m-1$, through to 1 occurs. For graph No. 13 in Fig 3.1, $\mathrm{RI}_2 = (12, 3)$ and $\mathrm{RI}_3 = (4, 4, 2)$: for smaller sets in the bipartition of qubit labels of the graph containing two qubits, there are twelve sets with a Schmidt rank of 2 and three sets with a Schmidt rank of 1. For smaller sets of three qubits, the Schmidt rank 3 occurs four times, 2 occurs four times and 1 occurs twice. This corresponds to the occurrences of different purities of reduced states calculated for the Concentratable Entanglement. Using Eq. (3.28), the rank index can be used to give the number of splits where the purity is $(2^{-m}, \ldots, 1)$ for bipartitions with a smaller set of m qubits. For any connected graph of seven or fewer vertices, the Concentratable Entanglement for $s = \mathcal{S}$ can be calculated using the results for the rank index in Table II of [17].

3. Graph states for repeaters. Azuma et al. [37] propose a quantum repeater design based on graph states; repeater stations create 'snowflake' graph states as shown in Fig. 3.2, to perform entanglement swapping and set up direct entanglement over larger distances. The inner 1st leaf qubits (grey) form a fully connected graph so there is a direct path between any two qubits. Each 1st leaf qubit is further connected to a single 2nd leaf qubit (black).

Consider a snowflake state of $2n$ qubits where the 1st leaf qubits have labels in the set $\mathcal{S}_{1\mathrm{st}} = \{1_1, 2_1, \ldots, n_1\}$ and the 2nd leaf qubit labels are $\mathcal{S}_{2\mathrm{nd}} = \{1_2, 2_2, \ldots, n_2\}$. Qubit a_2 is the 2nd leaf qubit paired with 1st leaf qubit a_1. The stabilizer generator for each 1st leaf qubit $a_1 \in \mathcal{S}_1$ is

$$S_{a_1} = X_{a_1} Z_{a_2} \prod_{b \in \mathcal{S}_1 \setminus \{a_1\}} Z_b. \tag{3.29}$$

Each 2nd leaf qubit $a_2 \in \mathcal{S}_2$ has a stabilizer generator of the form

$$S_{a_2} = X_{a_2} Z_{a_1}. \tag{3.30}$$

When measuring a 1st leaf qubit in the Z direction, the outcome -1 introduces a minus sign to the stabilizer generator for its 2nd leaf qubit partner and in the stabilizer generators for all other 1st leaf qubits, as they are all in the neighbourhood. For a 2nd leaf qubit, the measurement outcome -1 introduces a minus sign only to the stabilizer generator of its paired qubit in the 1st leaf. Therefore, if a pair $\{a_1, a_2\}$ is traced out, there are only two possible sets of stabilizer generators. The 1st leaf qubit stabilizer generators either all acquire a minus sign or they do not.

By allowing for at most one of the qubits in each pair $\{a_1, a_2\}$ to be traced out, the pattern in which minus signs are introduced results in each measurement outcome giving a unique set of stabilizer generators for the remaining qubits. $m \leq n$ non-paired qubits can be treated in this way. The purity of the reduced state left when tracing out these m qubits is 2^{-m}. Using this result to calculate each of the purities required, the Concentratable Entanglement for sets s of n qubits containing no pairings, including the sets containing exclusively 1st leaf or exclusively 2nd leaf qubits, is

$$C_{|G\rangle}(s) = 1 - \frac{1}{2^n} \sum_{m=0}^{n} \binom{n}{m} \frac{1}{2^m} = 1 - \left(\frac{3}{4}\right)^n. \tag{3.31}$$

This is the maximum Concentratable Entanglement possible for a set of n qubits within a graph state of $2n$ qubits. Therefore within a snowflake state, all of the 1st leaf qubits or all of the 2nd leaf qubits exhibit maximal entanglement with respect to the rest of the state.

4. Limits on overall entanglement. Concentratable Entanglement provides a measure of the overall entanglement of a state when applied to the set $\mathcal{S}$. There are theoretical bounds on the maximum and minimum values that the Concentratable Entanglement can take.

The minimum value of Concentratable Entanglement occurs when the purity of each possible reduced state is maximised. Since a connected graph represents an entangled pure state, any reduced state cannot be pure, excluding the reduced state containing no qubits where $\mathrm{Tr}\rho_\emptyset^2 = 1$. The maximum value each of these purities can take according to Theorem 1 is $1/2$, where there are two sets of stabilizer generators to describe the remaining qubits within the reduced state. The minimum value of Concentratable Entanglement for a graph state of n qubits

is therefore

$$\begin{aligned} C_{|G\rangle}(\mathcal{S}) &= 1 - \frac{1}{2^n}\left(\mathrm{Tr}\rho_{\emptyset}^2 + \mathrm{Tr}\rho_{\mathcal{S}}^2 + \sum_{i=1}^{n-1}\binom{n}{i}\frac{1}{2}\right) \\ &= \frac{1}{2} - \frac{1}{2^n}. \end{aligned} \tag{3.32}$$

This is the Concentratable Entanglement of the GHZ state [41]. The n qubit GHZ state is LU equivalent to the star graph and the complete graph, which take this value for Concentratable Entanglement.

If instead the purity of each reduced state is minimised, the Concentratable Entanglement will be maximised. It is not always possible to minimise the purity of all reduced states due to the structure of entanglement and the dependent relationships between different subsets of qubits. The purity of the reduced state of qubits in A or B is minimised when the number of sets of stabilizer generators is given by

$$k = 2^{\min(|A|,|B|)}. \tag{3.33}$$

This gives a new set of stabilizer generators for each measurement outcome when tracing out qubits, up to the number of measurement outcomes possible for the smaller set of A and B due to Eq. (3.16). Therefore the maximum value that the Concentratable Entanglement can achieve for a graph state of n qubits is

$$C_{|G\rangle}(\mathcal{S}) = 1 - \frac{1}{2^n}\sum_{j=0}^{n}\binom{n}{j}\frac{1}{2^{\min(j,n-j)}}. \tag{3.34}$$

Graph states that maximise the Concentratable Entanglement exist only for 2, 3, 5 and 6 qubits, and an example from each LU equivalence class is shown in Fig. 3.3. Trivially, a graph state of a single qubit satisfies Eq. (3.34), however it does not represent an entangled state and subsequently is of little interest. For graph states of 2 or 3 qubits, the maximum value of Concentratable Entanglement is equal to the minimum value, as the smaller (non-empty) bipartition always contains a single qubit, restricting all purities to the same value of $1/2$.

An absolutely maximally entangled (AME) state [74] has maximal entanglement in all bipartitions. If B is the smaller set containing j qubits in a bipartition (A, B), then the bipartition is maximally entangled if the reduced state of qubits in B can be written as the mixed state

$$\rho_B = \frac{1}{2^j} I_{2^j}. \tag{3.35}$$

The purity of this state is 2^{-j}. An AME state will achieve the maximum value of Concentratable Entanglement. The states of 2, 3, 5 and 6 qubits that maximise the Concentratable Entanglement are known AME states.

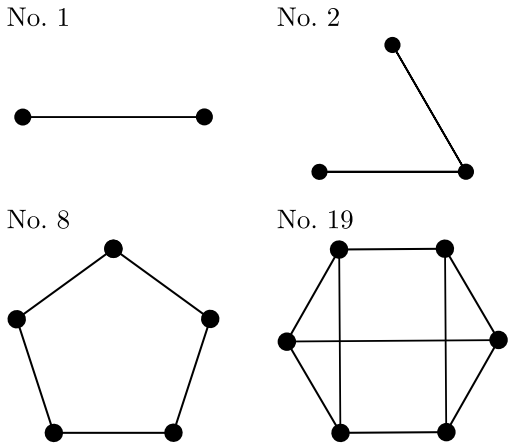

Figure 3.3: The LU classes of graph states, numbered according to [17, 72, 73], where the overall Concentratable Entanglement achieves the maximum theoretical value.

5. Graphs up to nine qubits. For graph states consisting of nine qubits or fewer, we have calculated the overall Concentratable Entanglement of the state, as shown in Fig. 3.4. The respective values of 0 and 1/4 for the Concentratable Entanglement of the unique graph states of 1 and 2 qubits are not shown. The theoretical maximum and minimum values of Concentratable Entanglement bound the area shaded in grey. Star states achieving the minimum Concentratable Entanglement, which are LU equivalent to GHZ states lie on the lower boundary of this area. The states with the greatest Concentratable Entanglement of each size are shown, and can be seen to achieve the maximum only for states of 3, 5 and 6 qubits.

Figure 3.4 also highlights the Concentratable Entanglement for linear and ring graph states. Linear cluster states of photons have been experimentally realised [75, 76]: an important step in developing the two dimensional clusters needed for MBQC and therefore their overall Concentratable Entanglement is shown. Ring states are similar to linear states although a further CZ operation is applied between the first and final qubits in the chain, thus completing a ring. Ring states have higher Concentratable Entanglement than linear states except for states of up to four qubits, where a ring and linear state are LU equivalent.

All of the overall Concentratable Entanglement values for graph states of nine qubits or fewer are shown in Fig. 3.4. Graph states within the same LU class will have the same overall Concentratable Entanglement, however using Concentratable Entanglement as a measure of the overall entanglement in a state is not sufficient to identify the LU class of a graph state, as the same value can occur for

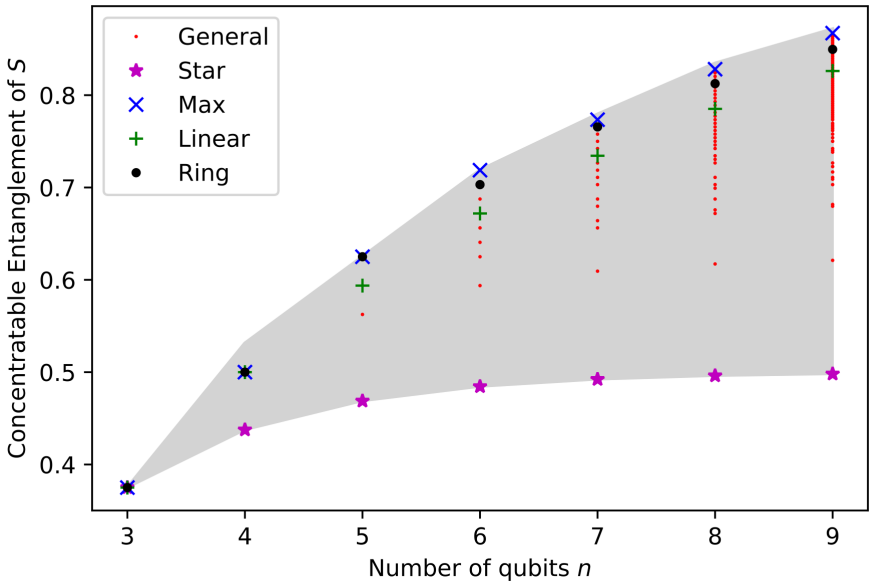

Figure 3.4: The possible values of overall Concentratable Entanglement of graph states of 3 to 9 qubits. Theoretical bounds on the Concentratable Entanglement define the area in grey. We consider special classes of states, which are given different markers, as shown in the legend.

more than one class. For example, for graph states of seven qubits, there are 26 LU equivalence classes, but only 16 possible values of Concentratable Entanglement. If Concentratable Entanglement is calculated using Eq. (3.1), the reduced state purities can be studied to identify the LU class of a state. However, if a quantum computer were used to perform a SWAP test, further calculations would be required, such as performing SWAP tests to calculate the Concentratable Entanglement for subsets of qubits within the state to identify the LU class from the entanglement structure.

The analysis of all graph states up to nine qubits was performed using Python and the networkx package [77] with graphs in graph6 format from the collections available at [78].

3.4 Discussion

We have presented a method for calculating the purity of reduced states and hence the Concentratable Entanglement for graph states entirely within the stabilizer

formalism, using only the stabilizer generators of a graph state. By evaluating the Concentratable Entanglement for different graph states we have found closed forms when considering a single qubit in any graph state and either the inner or outer leaf qubits in a snowflake state for use in a quantum repeater. We have also shown how Concentratable Entanglement relates to previous results regarding Schmidt rank and AME states. However the overall Concentratable Entanglement of graph states in different LU classes is shown to overlap in certain cases, suggesting that calculation of this version of the measure alone is insufficient to identify the entanglement structure of a graph state.

Though Concentratable Entanglement was introduced for pure qubit states, it may be possible to use it as an entanglement measure for pure qudit states. Further work could then look to extend the definition in terms of purities given in Eq. (3.1) to graph states of qudits. Extension of the SWAP test to qudits [79] may allow for calculation of Concentratable Entanglement via test outcomes when using a quantum computer in a similar manner to the qubit case. Qudit graph states [80–82] are stabilizer states for qudits of prime dimension d and allow for weighted or multiple edges. Reduced states could be found by considering all possible measurement outcomes, setting the stabilizer generators for measured qubits accordingly, and using the group structure of the stabilizer. The purity of the reduced state could again be calculated based on the number of unique sets of stabilizer generators.

It is unlikely that the result for calculating purities using stabilizer generators within the stabilizer formalism can be applied to hypergraphs. Like qudit graph states, hypergraphs [83–85] allow for weighted or repeated edges between the same qudits but hyperedges that can connect any number of qudits are introduced. The stabilizer generator for each qudit is given in terms of CZ gates on multiple qudits, which are not within the Pauli group. Therefore hypergraphs with hyperedges connecting more than two qudits are not true stabilizer states and do not allow for the group properties of a stabilizer to be used to find updated generators following a measurement.

More recently, upper and lower bounds on the Concentratable Entanglement for mixed states have been proposed [79, 86]. Even single qubit errors either in the generation or transmission of qubits within graph states can result in a mixed state. The extension of Concentratable Entanglement to mixed states could enable the study of effects such errors have on the entanglement within graph states, though it is unclear whether the stabilizer formalism could be used and whether it would offer a more efficient method to calculate these bounds.

Chapter 4

A Measurement Based Protocol for Two-Qubit Unitaries

When performing a quantum computation, the operations to enact the computation can be visualised using a quantum circuit, where each wire represents a single qubit to which unitary transformations are applied. To apply operations to an input state, a set of gates that can be physically implemented within an experimental set-up are required. Such a set is universal if some combination of gates from the set can be used to perform all possible operations needed for any quantum computation.

Another method to achieve universal quantum computation, as proven in [16], is through Measurement Based Quantum Computation (MBQC) using the one-way quantum computer [15]. The set-up requires a large entangled resource state and the computation then proceeds through a series of single-qubit measurements of qubits within this state. Most importantly within the context of this thesis, the resource state for MBQC is a graph state, and hence can be described using the stabilizer formalism.

The structure of the resource graph state is determined by the computation that is performed, with each column representing qubits that are measured within the same time step and the number of rows corresponding to the number of qubits within the input state of the computation. An example resource state is shown in Fig. 4.1. The process is one-way since measurement of a qubit within a graph state removes it from the graph, thus the resource state is consumed by performing a computation. The implementation is also feed-forward in nature, as adjustments to measurement bases are determined by the outcome of previous measurements within the procedure. The computation also results in byproduct operators, conditional on each measurement outcome, which act on the output state in the form of corrective Pauli operations due to the probabilistic nature of each measurement.

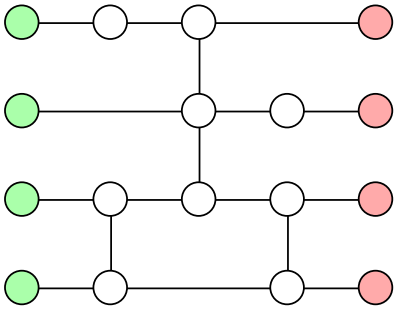

Figure 4.1: A lattice-like graph state that can be used as a resource state for MBQC. The qubits in green form a joint input state of four qubits. Qubits in red become the output state. The input and central qubits are measured in bases determined by the computation, with adjustments made due to measurement results at previous time steps in the preceding columns.

In practice, the graph state resource required for MBQC can be large and difficult to produce with current experimental capabilities. Though the theory also allows for the resource state to be produced in a rolling manner, where each column is only generated shortly before it is needed, this is unlikely to occur deterministically, risking destruction of the state and making operations performed up to this point redundant. Therefore, a process where a smaller resource graph state can be produced prior to commencing the single-qubit measurements is a necessity at present.

Here, we derive a measurement based protocol to implement a two-qubit unitary (up to local unitaries). The two-qubit input state for the unitary operation may be shared between two distinct parties who cannot perform joint operations. In MBQC, sharing a pre-existing graph state resource allows the two parties to perform components of the two-qubit unitary locally using single qubit measurements. The protocol is an adapted version of MBQC using the one-way quantum computer, since we require an enhanced resource state where Hadamard and phase gates are needed in addition to CZ operations on qubits that are prepared in the state $|+\rangle$. We describe each of the gates needed to implement the two-qubit operation, before combining them to determine the full resource state, and we then consider the impact of theoretical single-qubit Pauli measurements within the stabilizer formalism in order to reduce the number of qubits required. Throughout construction of the protocol, we keep track of the necessary byproduct operators and measurement basis adjustments that result from previous measurement outcomes.

4.1 Two-qubit Unitary

A two-qubit unitary transformation can be decomposed into eight local unitaries and three CNOT gates [87]. A CNOT gate acts on two qubits and applies a Pauli X (or bit flip) operation to the target qubit only when the control qubit is in the state $|1\rangle$.

$$\text{CNOT} = \begin{pmatrix} 1 & 0 & 0 & 0 \\ 0 & 1 & 0 & 0 \\ 0 & 0 & 0 & 1 \\ 0 & 0 & 1 & 0 \end{pmatrix}. \tag{4.1}$$

The CNOT gate is in the Clifford group and can be written as the product of Hadamard and CZ gates,

$$\text{CNOT} = H_t \text{CZ} H_t, \tag{4.2}$$

where t denotes that the Hadamard gates are applied to the target qubit.

Using circuit representation, the decomposition of the two-qubit unitary is

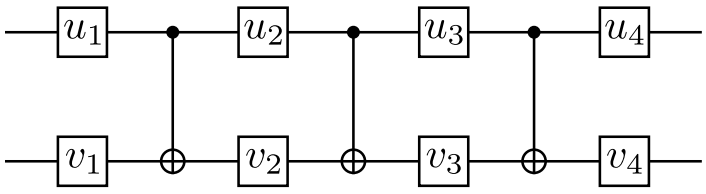

We focus on the central components of this circuit, where the two-qubit CNOT gates are not necessarily performed locally, for example if the joint input state of two qubits is held by two distinct parties. The local unitaries u_1 and v_1 can be performed by each party and are absorbed into the input for this section of the circuit and the local unitaries u_4 and v_4 can be accounted for in the output or can subsequently be performed by the two parties. In circuit representation, the implementation of the two-qubit unitary up to local unitaries requires seven gates

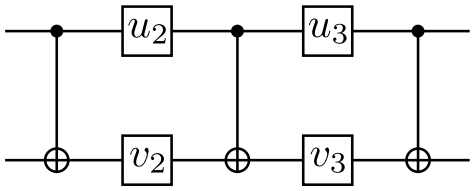

where [88]

$$u_2 = He^{ih_x X}, \quad v_2 = e^{ih_z Z},$$
$$u_3 = H\Phi, \quad v_3 = e^{-ih_y Z}.$$

Here H is the Hadamard gate that transforms between the Z and X basis states and Φ is the phase gate that enacts a rotation of π about the z axis as introduced in Eqs. (2.28) and (2.29) respectively. The exponentiated Pauli X and Z operators correspond to rotations around the x and z axes by angles $-2h_x$, $-2h_z$ and $2h_y$ respectively, where the parameters h_x, h_y and h_z are found in the decomposition of the two-qubit unitary [87, 88]. The two-qubit unitary, up to local unitaries u_1, v_1, u_4 and v_4, is

$$\mathcal{U} = \mathrm{CNOT}[H\Phi \otimes U_z(2h_y)]\mathrm{CNOT}[HU_x(-2h_x) \otimes U_z(-2h_z)]\mathrm{CNOT}. \tag{4.3}$$

The measurement based implementations of the gates required for the two-qubit unitary can be derived from their circuit representations following the method of Nielsen [89].

Hadamard Gate

The one-bit teleportation circuit [90] is used to teleport the state of a single qubit from one party to another.

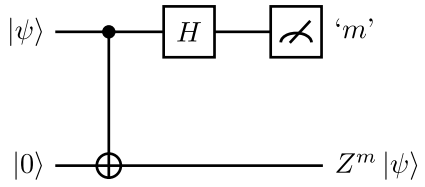

The procedure requires the second party to possess an ancillary qubit in the state $|0\rangle$, which is the target qubit in a joint CNOT operation between the qubits. Following this, the first party applies a Hadamard gate to their qubit and then performs a measurement in the computational basis, i.e. a Pauli Z measurement. This leaves the second qubit in the state $Z^m|\psi\rangle$, where $m \in \{0, 1\}$ is the outcome of the measurement. The measurement outcome can be classically communicated to the second party in order to perform a corrective Z operation if required, therefore resulting in the state $|\psi\rangle$.

By using the identity of Eq. (4.2), the CNOT gate can be replaced by Hadamard and CZ operations.

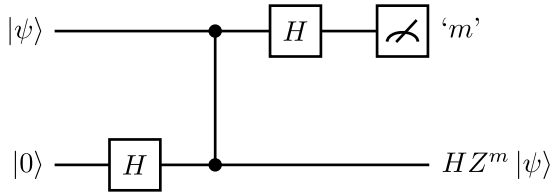

Applying a Hadamard gate to the state $|0\rangle$ is equivalent to using an input qubit in the state $|+\rangle$. This aligns the circuit with the set-up for MBQC because the

resource state of a single qubit in the state $|+\rangle$ is entangled with the input state by a CZ operation. The byproduct operator Z^m can be propagated through the Hadamard gate.

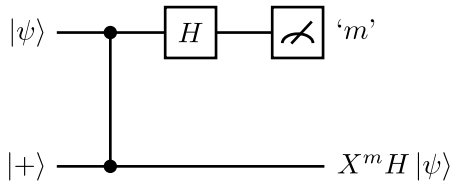

Rather than applying a Hadamard operation to the first qubit followed by a Z direction measurement, the measurement can instead be performed in the X basis, with outcomes 0 and 1 corresponding to the eigenstates $|+\rangle$ and $|-\rangle$ respectively. The circuit implements a Hadamard operation with byproduct operator X^m conditional on the measurement outcome.

The MBQC representation for a Hadamard operation on the state $|\psi\rangle$ is:

The single-qubit input is entangled by a CZ gate with a resource graph state containing one qubit and then measured in the X direction, resulting in an output state $X^m H\,|\psi\rangle$.

CNOT Gate

The measurement based implementation for a CNOT gate can be constructed using Eq. (4.2) and the above implementation of a Hadamard gate. Firstly, the target qubit undergoes a Hadamard operation using a single qubit resource state and an X basis measurement. The output of this operation and the control qubit are then entangled by a CZ gate, represented by an edge. Finally, the target qubit undergoes another Hadamard operation using a further resource qubit and a second X basis measurement.

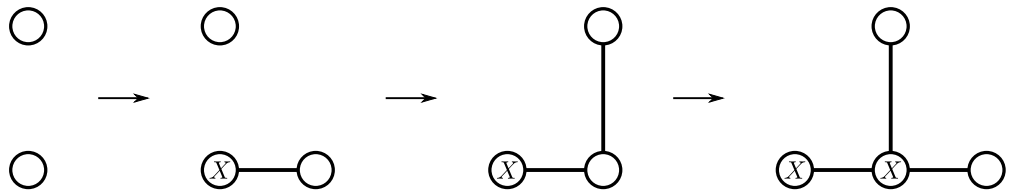

By performing the three required gates in turn, the output state is

$$X_t^{m_2} H_t \mathrm{CZ} X_t^{m_1} H_t\,|\psi\rangle\,, \tag{4.4}$$

where $m_1, m_2 \in \{0, 1\}$ are the two measurement outcomes respectively. To resolve this with a CNOT gate, the byproduct X^{m_1} can be propagated through the CZ and H operations so the resulting state is ‘

$$X_t^{m_2}(Z_c Z_t)^{m_1} H_t \mathrm{CZ} H_t \left|\psi\right\rangle = X_t^{m_2}(Z_c Z_t)^{m_1} \mathrm{CNOT} \left|\psi\right\rangle, \tag{4.5}$$

where c denotes a gate acting on the control qubit.

$H\Phi$ Operation

A $H\Phi$ operation, or a phase gate followed by a Hadamard gate, can be implemented by applying the circuit for a Hadamard gate to the input state $\Phi \left|\psi\right\rangle$.

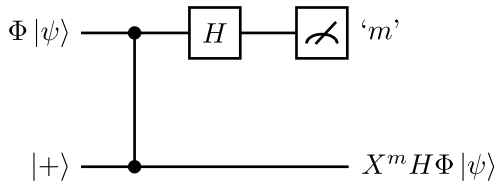

Since the CZ gate and phase gate commute, their order within the circuit can be swapped.

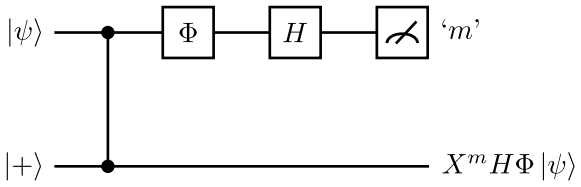

Instead of applying gates Φ and H to the input qubit then measuring in the Z basis, the measurement can instead be performed in the $\Phi^\dagger H Z H \Phi = -Y$ basis [89], with byproduct X^m. This can be replaced by a Y basis measurement, which is the same measurement with outcomes and eigenvalues interchanged, and the byproduct operator becomes $X^{m_1 \oplus 1}$. The MBQC representation is:

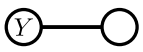

z-axis Rotation

A general rotation about the z-axis is $U_z(\theta) = e^{-i\theta Z/2}$. The known circuit to implement a Hadamard operation can be applied to the input state $U_z(\theta) \left|\psi\right\rangle$.

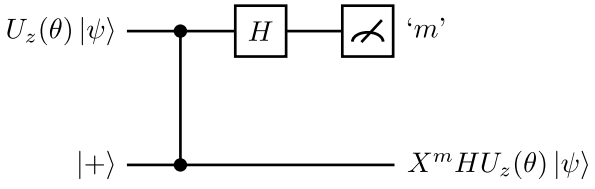

Similarly to the previous $H\Phi$ gate, the $U_z(\theta)$ operation commutes with the CZ gate and their order can be swapped.

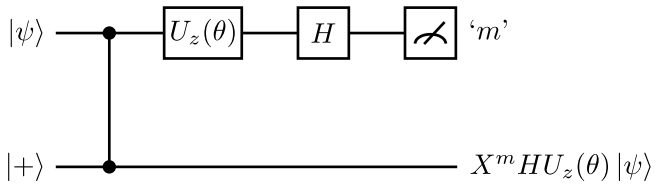

Rather than applying $U_z(\theta)$ and H prior to a Z basis measurement, the measurement can be performed in the basis [89]

$$\{U_z^\dagger(\theta)H\,|0\rangle\,, U_z^\dagger(\theta)H\,|1\rangle\} \equiv \left\{\frac{|0\rangle + e^{-i\theta}\,|1\rangle}{\sqrt{2}}, \frac{|0\rangle - e^{-i\theta}\,|1\rangle}{\sqrt{2}}\right\}, \tag{4.6}$$

where a global phase of $e^{i\theta/2}$ is ignored. This is the measurement $M(-\theta)$, where $M(\phi)$ denotes measurement in the basis

$$\left\{\frac{|0\rangle + e^{i\phi}\,|1\rangle}{\sqrt{2}}, \frac{|0\rangle - e^{i\phi}\,|1\rangle}{\sqrt{2}}\right\}. \tag{4.7}$$

However, performing the measurement $M(-\theta)$ applies $HU_z(\theta)$ (with byproduct X^m) so an additional Hadamard operation must be applied to the output. A further $|+\rangle$ qubit is entangled with the output qubit via CZ operation and an X basis measurement is performed. This results in the state

$$\begin{aligned} X^{m_2}HX^{m_1}HU_z(\theta)\,|\psi\rangle &= X^{m_2}Z^{m_1}HHU_z(\theta)\,|\psi\rangle \\ &= X^{m_2}Z^{m_1}U_z(\theta)\,|\psi\rangle\,, \end{aligned} \tag{4.8}$$

where $m_1, m_2 \in \{0, 1\}$ are the measurement outcomes in the order they are performed. The MBQC representation for the z-axis rotation is:

x-axis Rotation

A general x-axis rotation $U_x(\theta) = e^{-i\theta X/2}$ can be written as

$$U_x(\theta) = HU_z(\theta)H. \tag{4.9}$$

Therefore an x-axis rotation can be treated as a Hadamard gate followed by a $HU_z(\theta)$ operation. These are implemented by entangling the input state with a two qubit graph state resource and measuring the first qubit in the X basis, followed by the measurement $M(-\theta)$ on the second qubit. This is represented by:

However, the final state following these measurements is

$$\begin{aligned} X^{m_2} H U_z(\theta) X^{m_1} H \left|\psi\right\rangle &= X^{m_2} Z^{m_1} H U_z[(-1)^{m_1}\theta] H \left|\psi\right\rangle \\ &= X^{m_2} Z^{m_1} U_x[(-1)^{m_1}\theta] \left|\psi\right\rangle \end{aligned} \tag{4.10}$$

In order to perform the rotation $U_x(\theta)$, the measurement basis for the second qubit must be adapted to $M[-\theta(-1)^{m_1}]$, dependent on the outcome $m_1 \in 0, 1$ of the first measurement.

4.2 Measurement Based Implementation

Gates can be concatenated, where the output qubit for a completed operation becomes the input for the following gate [16]. The CZ gates between qubits can be applied prior to conducting any of the measurements, allowing for the resource graph state of 14 qubits to be prepared in advance of the measurements being performed [16]. By combining the gates required, the circuit for the two-qubit unitary $\mathcal{U}$ in Eq. (4.3) is equivalent to operations on a 16 qubit graph state [1].

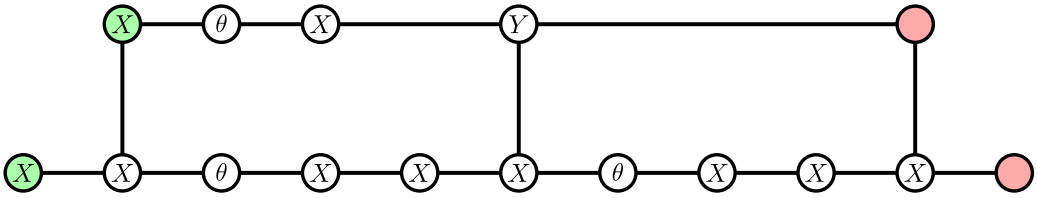

The qubits highlighted in green are the input qubits, which jointly are in the state $\left|\psi\right\rangle$ that the unitary operation is to be applied to. All 14 remaining qubits are prepared in the $\left|+\right\rangle$ state. The qubits highlighted in red are the output qubits, which (up to byproduct operators) are in the state $\mathcal{U}\left|\psi\right\rangle$ following the measurements on individual qubits. Each θ represents one of the angles $-2h_x$, $-2h_z$ and $2h_y$ within the decomposition of $\mathcal{U}$, with exact measurement bases stated in Section 4.4 once byproduct operators and previous measurement outcomes are accounted for.

Since a 16 qubit state is large and difficult to produce, efforts must be made to reduce the resource state required to perform the computation. Two neighbouring measurements in the X-direction can be treated as wires or equivalently as applying the identity operator and therefore the graph state required can be simplified to a state of 12 qubits.

[1] The 16 qubit state was put forward by Cosmo Lupo, Departimento di Fisica, Politecnico di Bari.

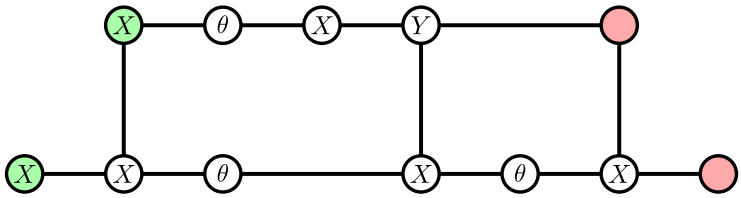

To keep track of the graph whilst subsequent measurements are performed, the qubits are numbered from 1 to 12. Qubits 1 and 2 are the input qubits and 11 and 12 are the output qubits.

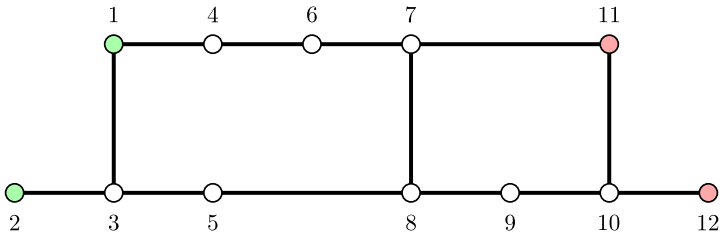

Pauli measurements can be performed prior to other operations within the measurement based set-up, since Pauli basis measurements enact Clifford operations, which can be performed in a single time step [16] [2]. In order to further reduce the resources required, rather than producing the full state of 12 qubits and performing these measurements, an updated initial resource state can be calculated, as though the measurements have been performed. Each theoretical measurement affects the topology of the remaining graph state and introduces operations on qubits neighbouring the measurement site. Therefore the remaining resource state does not consist only of $|+\rangle$ state qubits and CZ operations, so the procedure is an adapted form of MBQC on an enhanced resource state. A smaller resource state has a higher probability of being successfully created.

To use the stabilizer formalism to study the resulting operations on the resource state, assume qubits 1 and 2 are each in the state $|+\rangle$ [16]. When preparing the resource graph state, it is probable that operations will fail and multiple attempts will be required to successfully generate the state. Including the state $|\psi\rangle$ within this preparation would likely result in the state being destroyed or needing to be discarded when beginning another attempt at generation. Therefore the state $|\psi\rangle$ can be teleported into qubits 1 and 2 once the resource state is produced and prior to performing the required single qubit measurements, which can be done using the one-bit teleportation protocol [90] on both of the individual qubits within the joint state $|\psi\rangle$. The Pauli X measurements on qubits 1 and 2 are not considered

[2] By the Gottesman-Knill Theorem, these aspects of the computation can also be simulated on a classical computer.

in advance of 'real' measurements being performed so that they apply once the input state $|\psi\rangle$ is present.

The stabilizer generators for the graph state of 12 qubits are

$$\begin{aligned}
S_1 &= X_1 \quad Z_3 Z_4 \\
S_2 &= \quad X_2 Z_3 \\
S_3 &= Z_1 Z_2 X_3 \quad Z_5 \\
S_4 &= Z_1 \quad\quad X_4 \quad Z_6 \\
S_5 &= \quad\quad Z_3 \quad X_5 \quad\quad Z_8 \\
S_6 &= \quad\quad\quad Z_4 \quad X_6 Z_7 \\
S_7 &= \quad\quad\quad\quad Z_6 X_7 Z_8 \quad\quad Z_{11} \\
S_8 &= \quad\quad\quad Z_5 \quad Z_7 X_8 Z_9 \\
S_9 &= \quad\quad\quad\quad\quad Z_8 X_9 Z_{10} \\
S_{10} &= \quad\quad\quad\quad\quad\quad Z_9 X_{10} Z_{11} Z_{12} \\
S_{11} &= \quad\quad\quad\quad Z_7 \quad\quad Z_{10} X_{11} \\
S_{12} &= \quad\quad\quad\quad\quad\quad Z_{10} \quad X_{12}.
\end{aligned} \tag{4.11}$$

4.2.1 X direction Measurements

The outcome for each of the X measurements can be assumed to be 0 since it is a fictitious measurement, reducing the byproduct operators corresponding to these measurements. We refer to these measurements as fictitious since they are only being performed in theory in order to calculate the resulting state that the system collapses to, which is the actual state that will be produced. This is effectively post-selection of outcome 0. Therefore the state of the measured qubit a collapses to $|+\rangle$, associated with stabilizer generator X_a, and the qubit is removed from the graph. To measure a qubit a within a graph in the X direction, a neighbourhood qubit of a, i.e. $b \in n(a)$, is selected. Despite not actually performing the measurements, to respect the feed-forward nature of the one-way quantum computer, the selected qubit b will always be to the right of the measured qubit a within the graph state. Since all of the Pauli measurements can take place in a single time step, the order in which the fictitious measurements are considered corresponds to their numbering, with the X direction measurements prior to the Y direction measurement. Much like in the case of a Z direction measurement, there are multiple methods to approach the X direction measurements.

To visualise the effect of the measurement on a graph state, firstly the subgraph G_1 with edges between b and the other qubits in the neighbourhood of a is drawn. Next, the subgraph G_2 has edges between qubits that are in the neighbourhoods of both a and b. The final subgraph G_3 is constructed by drawing edges between

each qubit in a's neighbourhood and each qubit in b's neighbourhood. Lastly, the graph following the measurement is found by adding G_1, G_2 and G_3 to the original graph modulo 2 [49]. The stabilizer generators for the new graph state are found using Eq. (2.32) and applying the unitary $U_{x,+}$ for measurement outcome 0 [17]

$$U_{x,+} = (iZ_{b_0})^{1/2} \prod_{b \in n(a) - n(b_0) - \{b_0\}} Z_b. \tag{4.12}$$

It is perhaps simpler to to set the stabilizer for qubit a to X_a and using the group structure of the stabilizer to find new stabilizer generators that commute with X_a.

Measure Qubit 3: $a = 3$, $b = 5$. The subgraphs are:

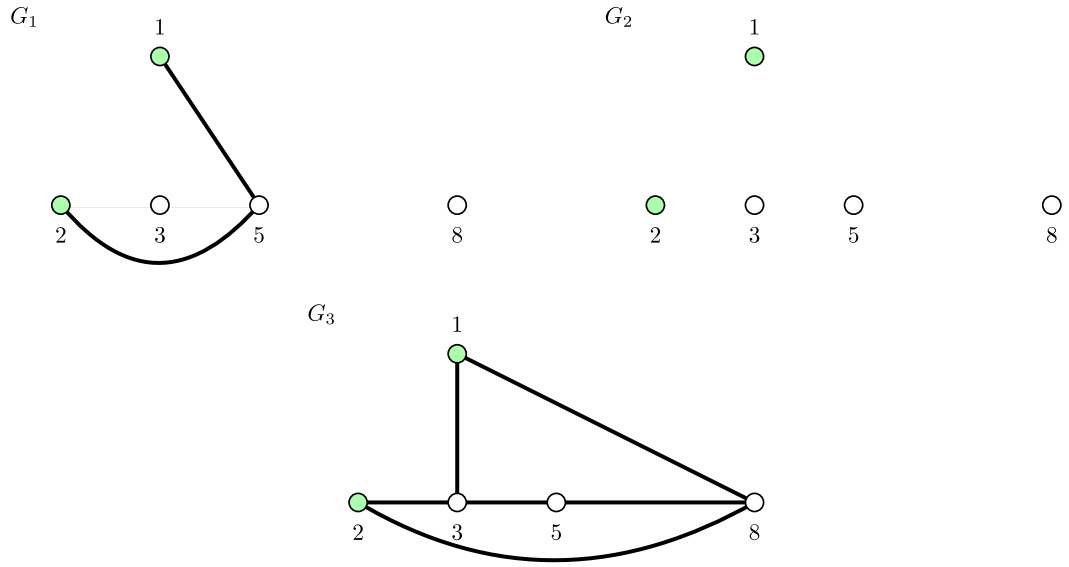

Following this measurement, the remaining graph state is:

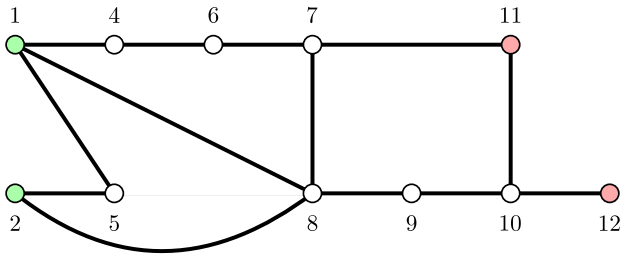

The updated stabilizer generator for qubit 3 is X_3. The generators for qubits 4, 6, 7, 8, 9, 10, 11 and 12 remain valid as they commute with X_3. Due to the group structure, multiplying S_3 by X_3 provides another generator — $S_5' = Z_1 Z_2 Z_5$, as

do the products $S_1S_5 = X_1Z_4X_5Z_8 = S_1'$, $S_2S_5 = X_2X_5Z_8 = S_2'$ and $S_8S_5' = Z_1Z_2Z_7X_8Z_9 = S_8'$. The full set of generators for the remaining state is

$$\begin{aligned}
S_1' &= X_1 \quad Z_4X_5 \quad\quad Z_8 \\
S_2' &= \quad X_2 \quad X_5 \quad\quad Z_8 \\
S_4' &= Z_1 \quad X_4 \quad Z_6 \\
S_5' &= Z_1Z_2 \quad Z_5 \\
S_6' &= \quad\quad Z_4 \quad X_6Z_7 \\
S_7' &= \quad\quad\quad Z_6X_7Z_8 \quad\quad Z_{11} \\
S_8' &= Z_1Z_2 \quad\quad Z_7X_8Z_9 \\
S_9' &= \quad\quad\quad\quad Z_8X_9Z_{10} \\
S_{10}' &= \quad\quad\quad\quad\quad Z_9X_{10}Z_{11}Z_{12} \\
S_{11}' &= \quad\quad\quad Z_7 \quad\quad Z_{10}X_{11} \\
S_{12}' &= \quad\quad\quad\quad\quad\quad Z_{10} \quad\quad X_{12}.
\end{aligned} \tag{4.13}$$

Writing out the set of stabilizer generators in full allows them to be easily compared to the form of Eq. (2.32) and it can be seen that these are the generators for the graph once qubit 3 is measured, with a Hadamard gate applied to qubit 5.

Measure Qubit 6: $a = 6$, $b = 7$. The subgraphs are:

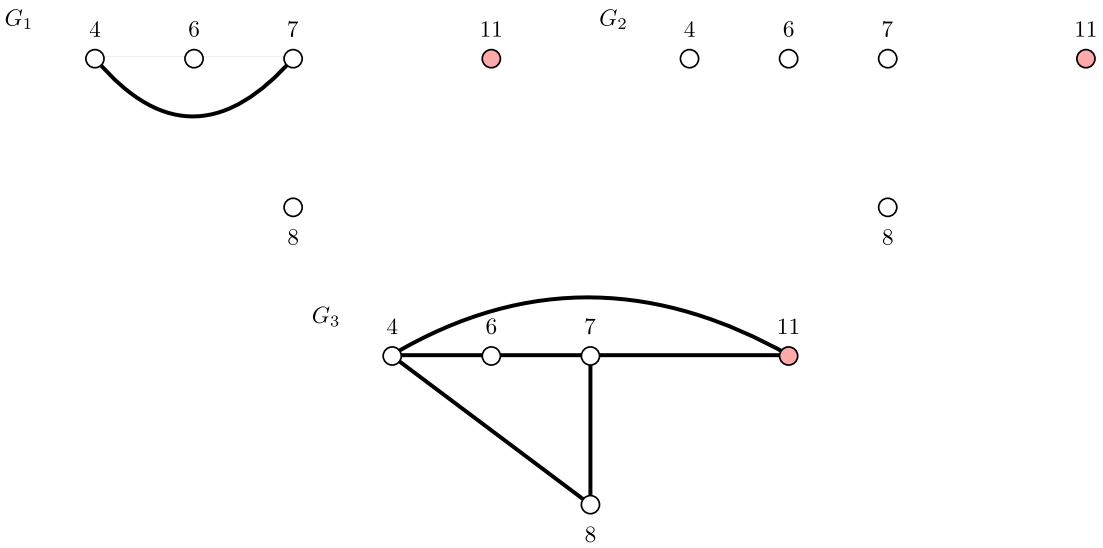

Following this measurement, the remaining graph state is:

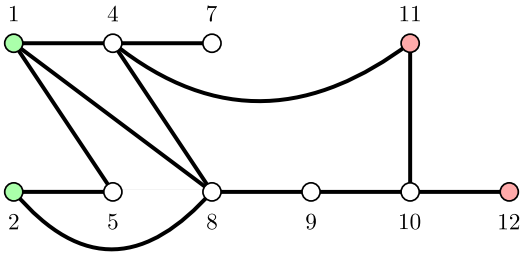

The generator for qubit 6 becomes X_6. Through manipulation of the existing generators, updated generators can be brought to the form of Eq. (2.32).

$$\begin{aligned}
S''_1 &= X_1 \quad Z_4X_5 \quad Z_8 \\
S''_2 &= \quad X_2 \quad X_5 \quad Z_8 \\
S''_4 &= Z_1 \quad X_4 \quad X_7Z_8 \qquad Z_{11} \\
S''_5 &= Z_1Z_2 \quad Z_5 \\
S''_7 &= \qquad Z_4 \quad Z_7 \\
S''_8 &= Z_1Z_2Z_4 \qquad X_8Z_9 \\
S''_9 &= \qquad\qquad Z_8X_9Z_{10} \\
S''_{10} &= \qquad\qquad\quad Z_9X_{10}Z_{11}Z_{12} \\
S''_{11} &= \qquad Z_4 \qquad\quad Z_{10}X_{11} \\
S''_{12} &= \qquad\qquad\quad Z_{10} \quad X_{12}
\end{aligned} \tag{4.14}$$

These are the stabilizer generators for the remaining graph state of 10 qubits where a Hadamard operation is applied to qubits 5 and 7.

Measure Qubit 8: $a = 8$, $b = 9$. The subgraphs are:

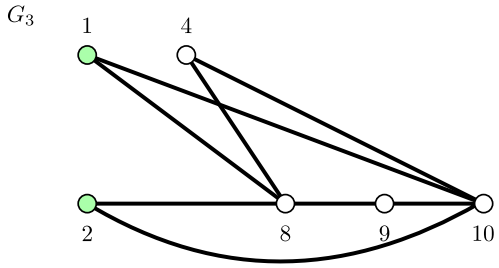

Following this measurement, the remaining graph state is:

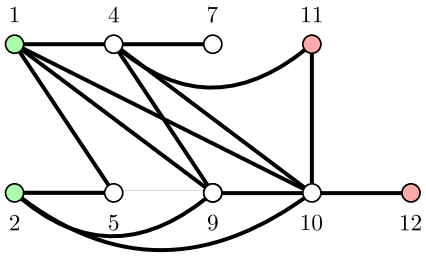

By tracking the state using the stabilizer formalism, the measurement applies a Hadamard operation to qubit 9, in addition to the previous Hadamard operations on qubits 5 and 7. The stabilizer generators are

$$\begin{aligned}
\hat{S}_1 &= X_1 \quad Z_4 X_5 \quad X_9 Z_{10} \\
\hat{S}_2 &= \quad X_2 \quad X_5 \quad X_9 Z_{10} \\
\hat{S}_4 &= Z_1 \quad X_4 \quad X_7 X_9 Z_{10} Z_{11} \\
\hat{S}_5 &= Z_1 Z_2 \quad Z_5 \\
\hat{S}_7 &= \qquad Z_4 \quad Z_7 \\
\hat{S}_9 &= Z_1 Z_2 Z_4 \qquad Z_9 \\
\hat{S}_{10} &= Z_1 Z_2 Z_4 \qquad\quad X_{10} Z_{11} Z_{12} \\
\hat{S}_{11} &= \qquad Z_4 \qquad\quad Z_{10} X_{11} \\
\hat{S}_{12} &= \qquad\qquad\quad Z_{10} \quad X_{12}.
\end{aligned} \tag{4.15}$$

Measure Qubit 10: $a = 10$, $b = 12$. The subgraphs are:

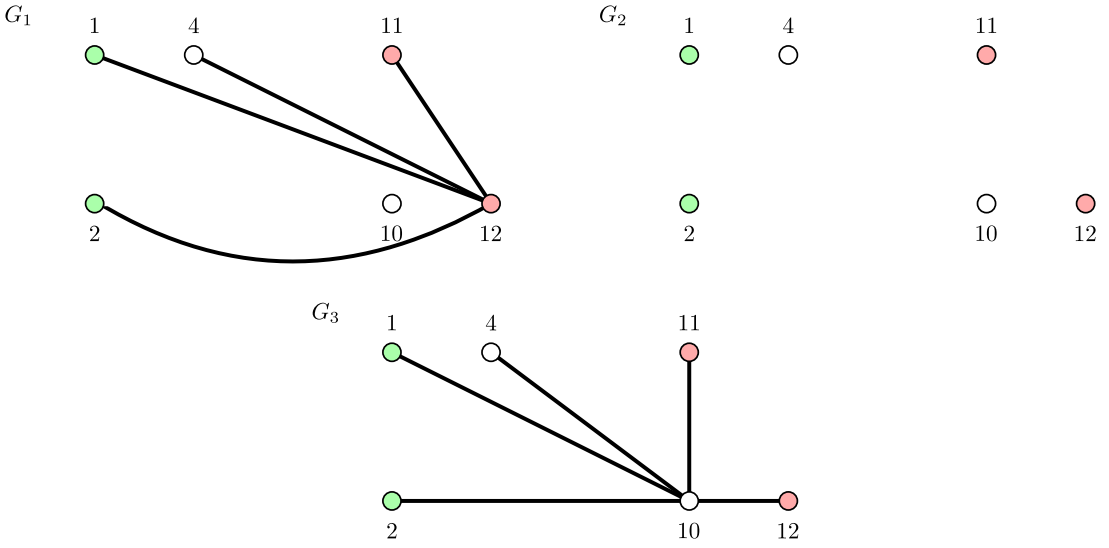

Following this measurement, the remaining graph state is:

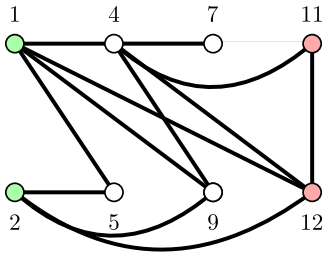

Using the stabilizer formalism, the generator for qubit 10 is set to X_{10}.

$$
\begin{aligned}
\check{S}_1 &= X_1 \quad Z_4 X_5 \quad X_9 \quad X_{12} \\
\check{S}_2 &= \quad X_2 \quad X_5 \quad X_9 \quad X_{12} \\
\check{S}_4 &= Z_1 \quad X_4 \quad X_7 X_9 Z_{11} X_{12} \\
\check{S}_5 &= Z_1 Z_2 \quad Z_5 \\
\check{S}_7 &= \quad Z_4 \quad Z_7 \\
\check{S}_9 &= Z_1 Z_2 Z_4 \quad Z_9 \\
\check{S}_{11} &= \quad Z_4 \quad X_{11} X_{12} \\
\check{S}_{12} &= Z_1 Z_2 Z_4 \quad Z_{11} Z_{12}
\end{aligned}
\tag{4.16}
$$

The generators for the remaining qubits correspond to the graphical representation of the state where a Hadamard is applied to qubit 12 in addition to qubits 5, 7 and 9.

4.2.2 Y direction Measurement

For a Y direction measurement, the subgraph of the measured qubit and its neighbours is inverted [49]. The outcome can be assumed to be 1 to reduce the byproduct operators, and the state of the measured qubit a collapses to the state $|-i\rangle$, associated with stabilizer generator $-Y_a$. The unitary associated with outcome 1 is [17]

$$U_{y,-} = \prod_{b \in n(a)} (iZ_b)^{1/2}, \tag{4.17}$$

however it is again favourable to utilise the group structure of the stabilizer to find updated stabilizer generators, rather than applying $U_{y,-}$ to the generator in the form of Eq. (2.32) for each vertex in the visual representation of the graph state following the measurement.

Measure Qubit 7: By inverting the subgraph between qubits 4 and 7, the edge between these qubits is removed from the graph and the remaining graph state is:

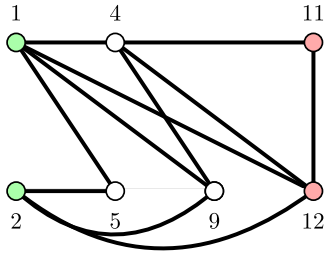

Figure 4.2: The graph state required to perform the two qubit unitary. A Hadamard operation must be applied to qubits 5, 9 and 12 and a phase gate to qubit 4.

Following this measurement, the set of stabilizer generators for the remaining qubits within the graph state is

$$\begin{aligned}
\tilde{S}_1 &= X_1 \quad Z_4X_5X_9 \quad X_{12} \\
\tilde{S}_2 &= \quad X_2 \quad X_5X_9 \quad X_{12} \\
\tilde{S}_4 &= Z_1 \quad Y_4 \quad X_9Z_{11}X_{12} \\
\tilde{S}_5 &= Z_1Z_2 \quad X_5 \\
\tilde{S}_9 &= Z_1Z_2Z_4 \quad Z_9 \\
\tilde{S}_{11} &= \quad Z_4 \quad X_{11}X_{12} \\
\tilde{S}_{12} &= Z_1Z_2Z_4 \quad Z_{12}.
\end{aligned} \tag{4.18}$$

These are the stabilizer generators for the graph state shown in Fig. 4.2, where a Hadamard gate has been applied to qubits 5, 9 and 12, and a phase gate Φ is applied to qubit 4.

4.3 Byproduct Operators

The graph state from Fig. 4.2 with Hadamard and phase corrections is set-up. Pauli X measurements are performed on input qubits 1 and 2 and the measurements on qubits 4, 5 and 9 are $M(-\theta_4(-1)^{m_1})$, $M(-\theta_5)$ and $M(-\theta_9)$, where $\theta_4 = -2h_x$, $\theta_5 = -2h_z$ and $\theta_9 = 2h_y$. This results in the output state

$$\begin{aligned}\mathrm{CNOT}[H\Phi \otimes Z_t^{m_9} U_z(\theta_9)]\mathrm{CNOT} \\ [HX_c^{m_4} Z_c^{m_1} U_x(\theta_4) \otimes Z_t^{m_5} U_z(\theta_5)_t][Z_c^{m_2} \otimes Z_t^{m_2}]\mathrm{CNOT}\,|\psi\rangle\,,\end{aligned} \tag{4.19}$$

where c and t denote the first and second qubit within the output state (these are the roles each qubit would have as control or target qubit within the applied CNOT gates). The outcomes 0 for X direction measurements and 1 for Y direction measurements accounted for in the set-up of the resource state ensure that the byproduct operators are reduced. For example, the full byproduct for the first CNOT gate is $Z_c^{m_2} \otimes X_t^{m_3} Z_t^{m_2}$, but since $m_3 = 0$ when considering the X basis measurement of qubit 3, the term $X_t^{m_3}$ has no effect.

The byproduct operators can be propagated through the state to apply only to the output qubits following the measurements. The following relations are required [16, 91]

$$\begin{aligned} HX = ZH, \quad HZ = XH, \\ \Phi X = Y\Phi, \quad \Phi Z = Z\Phi, \\ U_z(\phi)X = XU_z(-\phi), \quad U_x(\phi)Z = ZU_x(-\phi), \\ \mathrm{CNOT}Z_c = Z_c\mathrm{CNOT}, \quad \mathrm{CNOT}X_c = X_cX_t\mathrm{CNOT}, \\ \mathrm{CNOT}Z_t = Z_cZ_t\mathrm{CNOT}, \quad \mathrm{CNOT}X_t = X_t\mathrm{CNOT}. \end{aligned}$$

To show how the byproduct operators propagate, firstly they are brought up to the second CNOT gate

$$\begin{aligned}\mathrm{CNOT}[H\Phi \otimes Z_t^{m_9} U_z(\theta_9)]\mathrm{CNOT} \\ [Z_c^{m_4} X_c^{m_1 \oplus m_2} HU_x(\theta_4(-1)^{m_2}) \otimes Z_t^{m_2 \oplus m_5} U_z(\theta_5)]\mathrm{CNOT}\,|\psi\rangle\,.\end{aligned}$$

Next, the byproducts are brought through the second CNOT gate

$$\begin{aligned}\mathrm{CNOT}[H\Phi Z_c^{m_2 \oplus m_4 \oplus m_5} X_c^{m_1 \oplus m_2} \otimes Z_t^{m_9} U_z(\theta_9) X_t^{m_1 \oplus m_2} Z_t^{m_2 \oplus m_5}] \\ \mathrm{CNOT}[HU_x(\theta_4(-1)^{m_2}) \otimes U_z(\theta_5)]\mathrm{CNOT}\,|\psi\rangle\,.\end{aligned}$$

Then the byproduct operators are collected up to the third CNOT gate

$$\mathrm{CNOT}[X_c^{m_1 \oplus m_4 \oplus m_5} Z_c^{m_1 \oplus m_2} H\Phi \otimes X_t^{m_1 \oplus m_2} Z_t^{m_2 \oplus m_5 \oplus m_9} U_z(\theta_9(-1)^{m_1 \oplus m_2})] \\ \mathrm{CNOT}[HU_x(\theta_4(-1)^{m_2}) \otimes U_z(\theta_5)]\mathrm{CNOT}\,|\psi\rangle\,.$$

Finally, the byproduct operators are brought through the third CNOT gate so that they act only on the output qubits following all the necessary operations to apply the two-qubit unitary

$$[X_c^{m_1 \oplus m_4 \oplus m_5} Z_c^{m_1 \oplus m_5 \oplus m_9} \otimes X_t^{m_2 \oplus m_4 \oplus m_5} Z_t^{m_2 \oplus m_5 \oplus m_9}] \\ \mathrm{CNOT}[H\Phi \otimes U_z(\theta_9(-1)^{m_1 \oplus m_2})]\mathrm{CNOT}[HU_x(\theta_4(-1)^{m_2}) \otimes U_z(\theta_5)]\mathrm{CNOT}\,|\psi\rangle\,.$$

Comparing this output to $\mathcal{U}$ in Eq. (4.3), the two-qubit unitary is applied up to the byproduct operators if the measurement bases of qubits 4 and 9 are adjusted following the measurements of qubits 1 and 2. An additional factor of $(-1)^{m_2}$ is required in the measurement of qubit 4, so the measurement is $M(-\theta_4(-1)^{m_1 \oplus m_2})$. Similarly, the measurement of qubit 9 is updated to $M(-\theta_9(-1)^{m_1 \oplus m_2})$.

4.4 Summary

The protocol to apply $\mathcal{U}$ given by Eq. (4.3) to a two-qubit state $|\psi\rangle$ is as follows:

- Prepare the state represented by the graph

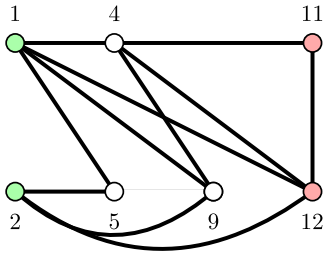

  where vertices represent qubits in the state $|+\rangle$ and edges denote CZ operations between qubits. Qubits 1 and 2 are jointly in the input state $|\psi\rangle$, though this may be achieved by teleporting in the state following the full process of resource state preparation.

- Apply a Hadamard operation H to qubits 5, 9 and 12 and a phase gate Φ to qubit 4 in the graph state.

- Measure qubits 1 and 2 in the Pauli X direction. Record the outcomes as m_1 and m_2.
- Perform measurements on qubits 4, 5 and 9 of $M(2h_x(-1)^{m_1 \oplus m_2})$, $M(2h_z)$ and $M(-2h_y(-1)^{m_1 \oplus m_2})$ respectively. $M(\phi)$ represents a measurement in the basis
$$\left\{ \frac{|0\rangle + e^{i\phi}|1\rangle}{\sqrt{2}}, \frac{|0\rangle - e^{i\phi}|1\rangle}{\sqrt{2}} \right\}.$$
- The joint state of qubits 11 and 12 is
$$[X^{m_1 \oplus m_4 \oplus m_5} Z^{m_1 \oplus m_5 \oplus m_9} \otimes X^{m_2 \oplus m_4 \oplus m_5} Z^{m_2 \oplus m_5 \oplus m_9}] \mathcal{U} |\psi\rangle . \quad (4.20)$$

We have derived a protocol for applying a two-qubit unitary using an adapted version of MBQC, wherein the resource state is prepared using CZ operations on single qubits in the state $|+\rangle$, as allowed in the definition of graph states, but with additional Hadamard and phase gates required. Once this state is prepared, the standard process of MBQC resumes, with single qubit measurements applied and feed-forward basis adjustments being made once previous measurement outcomes are accounted for.

Though the Pauli X measurements are treated in the stabilizer formalism by assuming the input state is $|+\rangle \otimes |+\rangle$, the protocol still applies the operation $\mathcal{U}$ up to byproduct operators for a general two qubit input state. To truly apply a general two-qubit unitary of the form $(u_4 \otimes v_4)\mathcal{U}(u_1 \otimes v_1)$, the local unitaries u_1 and v_1 can be applied to the input prior to teleporting the state $|\psi\rangle$ into qubits 1 and 2 and performing the required measurements. The operators u_4 and v_4 can be accounted for in interpretation of the output including the necessary byproduct operators, or can be undertaken locally once the Pauli corrections are applied.

An experimental demonstration of the implementation of $\mathcal{U}$ using the seven qubit resource state with five single-qubit measurements would be an important stage in being able to perform general two-qubit unitaries. Producing a seven qubit graph state is within current experimental capabilities. Members of the Laing research group at Quantum Engineering Technology (QET) Labs, University of Bristol, including Emilien Lavie, Molly Thomas, Imogen Forbes, Naomi Solomons and Patrick Yard are investigating on-chip implementation of the protocol.

Chapter 5

Graph States from Spin-Photon Interactions

Large graph states consisting of only photons have a multitude of applications, with examples including MBQC [15, 16, 89] and quantum repeaters [24, 25, 36, 37], due to the vital quantum resource provided by entanglement contained in such states. From a theoretical perspective, the appeal of graph states is boosted by their concise mathematical description using the stabilizer formalism and their graphical representation. Therefore the ability to be able to produce large photonic graph states efficiently is highly desirable.

Since, in general, photons do not interact with one another, the interaction between photons and a single-electron spin within a cavity can be used as a means to generate entangled states. The spin-photon interaction has applications within quantum networks [18], for example to enact quantum gates [92], for quantum teleportation and entanglement swapping [93] or for syndrome measurements in QEC [94]. A scheme to utilise spin-photon interactions as a photon entangler was proposed in [43], where the interaction can induce a phase shift of $\varphi = \pi/2$ depending on the state of both the photon and single-electron spin. This interaction combined with subsequent measurements of the spin can produce graph states and GHZ style states deterministically.

Here, we instead focus on a set-up in which the phase shift induced by spin-photon interactions is constrained by $0 < \varphi < \pi/2$. We show that we can produce heralded Bell pairs probabilistically using the interaction and measurement of the spin and describe a layered scheme to generate larger photonic GHZ style states probabilistically. We utilise the stabilizer formalism to track the interaction and the following measurements although it cannot be utilised in full due to the non-Clifford nature of the state evolution.

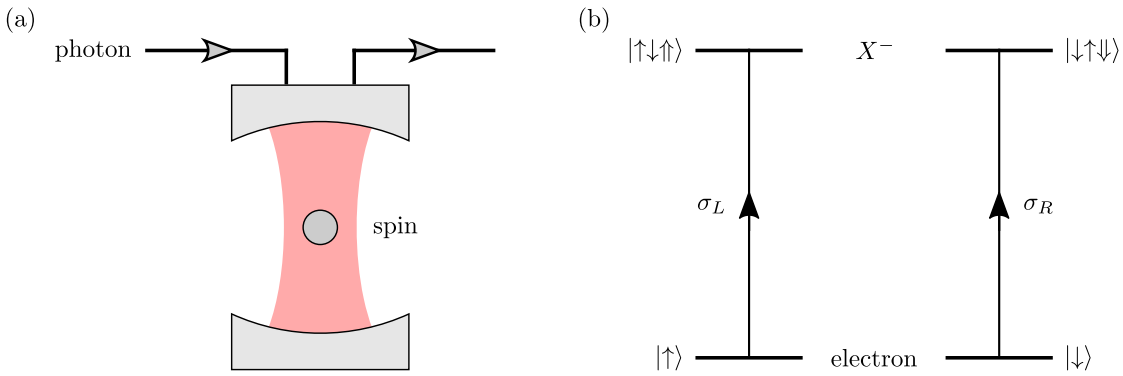

Figure 5.1: (a): A single photon is sent into and reflects out of a cavity containing a single-electron spin in a quantum dot. (b): The optical transitions of a negatively charged exciton (X^-) for left (σ_L) and right (σ_R) circularly polarized incident photons.

5.1 The Interaction

A single-electron spin in a quantum dot is contained within a microcavity as shown in Fig. 5.1(a), in a similar set-up to the scheme given by Hu et al. in [42] and [43]. The cavity is single-sided, allowing light to be reflected out of the cavity, but not transmitted. Light, treated as single photons, is sent in to the cavity to interact with the single-electron spin. This interaction induces phase shifts dependent on the states of both the photon and the spin.

A quantum dot is a three dimensional confinement of electrons such that the possible energy levels are discretised and may be constructed from a layer of one semiconductor within another such as InGaAs within GaAs. Consider a quantum dot containing a single excess electron in the spin state $|\uparrow\rangle$ or $|\downarrow\rangle$. The electron may absorb an incident photon, exciting it to a state with higher energy and hence it transitions from the valence band to the conduction band. This leaves a positively charged electron hole within the valence band, which can lie in the spin state $|\Uparrow\rangle$ or $|\Downarrow\rangle$. A negatively charged exciton X^- can be formed by this excitation, made up of two electrons and the electron hole together in a bound state. Fig. 5.1(b) show an energy level diagram for the optical transitions of X^- in the quantum dot. An electron in the state $|\uparrow\rangle$ is only excited by left circularly polarized light and similarly an electron in the state $|\downarrow\rangle$ is only excited by right circularly polarized light.

The cavity is said to be hot if the quantum dot couples to the cavity due to the optical transitions of the exciton, and cold if coupling does not occur or is much reduced. In the case of a hot cavity, interaction results in a phase shift of φ_h.

This occurs if the photon is left circularly polarized and the spin state is $|\uparrow\rangle$, or if the photon is right circularly polarized and the spin state is $|\downarrow\rangle$. Similarly, a cold cavity induces a phase shift of φ_0, which is the case if the photon is left circularly polarized and the spin state is $|\downarrow\rangle$, or if the photon is right circularly polarized and the spin state is $|\uparrow\rangle$. Assume, as in [42, 43], that the reflection coefficients for hot and cold cavities are equal (and ideally $\simeq 1$). Let $\varphi = \varphi_h - \varphi_0$. Thus the interaction is described up to a global phase of $e^{i\varphi_0}$ by the phase shift operator

$$U(\varphi) = e^{i\varphi(|L\rangle\langle L|\otimes|\uparrow\rangle\langle\uparrow|+|R\rangle\langle R|\otimes|\downarrow\rangle\langle\downarrow|)}. \tag{5.1}$$

Therefore, depending on the input state of the photon and single-electron spin, the phase shift operator transforms the state according to:

$$\begin{aligned} |L,\uparrow\rangle &\to e^{i\varphi}\,|L,\uparrow\rangle\,, \qquad |L,\downarrow\rangle \to |L,\downarrow\rangle\,, \\ |R,\uparrow\rangle &\to |R,\uparrow\rangle\,, \qquad |R,\downarrow\rangle \to e^{i\varphi}\,|R,\downarrow\rangle\,. \end{aligned} \tag{5.2}$$

Such a set-up can be used to generate multiparticle GHZ states and graph states consisting of photons through repeated interactions and subsequent measurements of the spin when the angle of the phase shift is $\varphi = \pi/2$ [42, 43], achieved through frequency detuning. If instead, the phase shift is constrained by $0 \leq \varphi < \pi/2$, which may be the case due to experimental limitations making it difficult to produce stronger interactions in the system, or due to an alternative set-up resulting in the same phase shift operator as Eq. (5.1), it is still possible to generate graph states probabilistically. This proposed scheme will be explored in part using the stabilizer formalism, requiring bases for both the photon and spin components of the interaction.

5.2 Spin-Photon Interaction

The Hilbert space for the interaction of a single photon and the spin is $\mathcal{H} = \mathcal{H}_p \otimes \mathcal{H}_s$. The computational basis for $\mathcal{H}_p$ is $\{|0\rangle_p, |1\rangle_p\}$, physically realised by a circularly polarized photon

$$|0\rangle_p \equiv |L\rangle\,, \quad |1\rangle_p \equiv |R\rangle\,. \tag{5.3}$$

In similar fashion, the computational basis for $\mathcal{H}_s$ is $\{|0\rangle_s, |1\rangle_s\}$, physically realised by a spin up or spin down electron

$$|0\rangle_s \equiv |\uparrow\rangle\,, \quad |1\rangle_s \equiv |\downarrow\rangle\,. \tag{5.4}$$

Each basis has a set of Pauli operators, enabling the phase shift operator of Eq. (5.1) to be written as

$$U(\varphi) = e^{i\varphi(Z_pZ_s+\mathbb{I})/2}. \tag{5.5}$$

The cavity shown in Fig. 5.1 is prepared with the electron in the superposition state $|+\rangle_s = (|\uparrow\rangle + |\downarrow\rangle)/\sqrt{2}$; the state stabilized by X_s. The single photon that enters the cavity to interact with the spin is also prepared in a superposition state, $|+\rangle_p = (|L\rangle + |R\rangle)/\sqrt{2}$, which in turn is stabilized by X_p. The overall state of the system prior to any interaction is

$$|+\rangle_p \otimes |+\rangle_s = \frac{1}{2}(|L,\uparrow\rangle + |L,\downarrow\rangle + |R,\uparrow\rangle + |R,\downarrow\rangle), \tag{5.6}$$

with stabilizer generators X_p and X_s.

Following the interaction, the photon is reflected out of the cavity and the overall state is

$$U(\varphi)(|+\rangle_p \otimes |+\rangle_s) = \frac{1}{2}(e^{i\varphi}|L,\uparrow\rangle + |L,\downarrow\rangle + |R,\uparrow\rangle + e^{i\varphi}|R,\downarrow\rangle). \tag{5.7}$$

To find the stabilizer generators for this state, the pre-interaction generators are updated according to $U(\varphi)X_pU^\dagger(\varphi)$ and $U(\varphi)X_sU^\dagger(\varphi)$. These new generators can be calculated using the Baker-Campbell-Hausdorff Formula

$$e^A B e^{-A} = B + [A,B] + \frac{1}{2!}[A,[A,B]] + \frac{1}{3!}[A,[A,[A,B]]] + \dots \tag{5.8}$$

for $A = i\varphi(Z_pZ_s + \mathbb{I})/2$ and $B \in \{X_p, X_s\}$. This results in the new stabilizer generators

$$\begin{aligned} X_p &\to X_p\cos(\varphi) - Y_pZ_s\sin(\varphi), \\ X_s &\to X_s\cos(\varphi) - Z_pY_s\sin(\varphi). \end{aligned} \tag{5.9}$$

There are three cases of interest:

- $\varphi = 0$. The stabilizer generators are X_p and X_s. As the interaction does not result in a phase shift, or any change to the input state, the generators remain unchanged.

- $\varphi = \pi/2$. The stabilizer generators become $-Y_pZ_s$ and $-Z_pY_s$. These are the generators for the maximally entangled graph state between the photon and spin with $S^\dagger$ applied to each particle in the relevant basis, where S is the phase gate. The phase shift operator can be written as $U(\pi/2) = i(S_p^\dagger \otimes S_s^\dagger)\mathrm{CZ}$, which is in the Clifford group and thus produces a stabilizer state. This result is expected, as for this value of φ, the interaction produces maximally entangled states [42, 43].

- $0 < \varphi < \pi/2$. The stabilizer generators are no longer within the Pauli group as the phase shift operator is not a Clifford operator and the state is not a true stabilizer state. The interaction results in a non-maximally entangled state with generators weighted between the generators for the separable state and the maximally entangled state, with weights of $\cos(\varphi)$ and $\sin(\varphi)$ respectively.

5.3 Multiple Interactions

It would appear that a simple solution to ensure that a maximally entangled state is produced between the photon and spin even when $\varphi \ll \pi/2$ would be to allow for the photon to enter the cavity and interact multiple times. For n interactions this would result in a phase shift of $n\varphi$, which could be repeated until the phase shift was $\pi/2$. However, it is usually not possible to send the same photon into the cavity to interact over and over again due to the one-directional routing within experimental set-ups and the accumulation of noise.

In order to use the set-up to generate photonic graph states, multiple photons must enter and interact with the single-electron spin inside the cavity. The simplest case to consider is where two photons interact with the spin successively within the decoherence time of the spin.

The photons, labelled p_1 and p_2, are each prepared in the photonic $|+\rangle$ state and are associated with stabilizer generators X_{p_1} and X_{p_2} respectively. The spin is again prepared in the state $|+\rangle_s$, with stabilizer generator X_s. Each interaction is described by a phase shift operator, $U_1(\varphi) = e^{i\varphi(Z_{p_1}Z_s+\mathbb{I})/2}$ and $U_2(\varphi) = e^{i\varphi(Z_{p_2}Z_s+\mathbb{I})/2}$. Applying U_1 and U_2 to the stabilizer generators gives the post-interaction generators as

$$\begin{aligned} X_{p_1} &\to X_{p_1}\cos(\varphi) - Y_{p_1}Z_s\sin(\varphi), \\ X_{p_2} &\to X_{p_2}\cos(\varphi) - Y_{p_2}Z_s\sin(\varphi), \\ X_s &\to X_s\cos^2(\varphi) - (Z_{p_1}Y_s + Z_{p_2}Y_s)\sin(\varphi)\cos(\varphi) - Z_{p_1}Z_{p_2}X_s\sin^2(\varphi). \end{aligned} \tag{5.10}$$

These stabilize the post-interaction state

$$\begin{aligned} U_2U_1(|+\rangle_{p_1}\otimes|+\rangle_{p_2}\otimes|+\rangle_s) = \frac{1}{2\sqrt{2}}(e^{2i\varphi}|LL\uparrow\rangle + |LL\downarrow\rangle + e^{i\varphi}|LR\uparrow\rangle + e^{i\varphi}|LR\downarrow\rangle \\ + e^{i\varphi}|RL\uparrow\rangle + e^{i\varphi}|RL\downarrow\rangle + |RR\uparrow\rangle + e^{2i\varphi}|RR\downarrow\rangle). \end{aligned} \tag{5.11}$$

To produce a graph state between the two photons in the case where $0 < \varphi < \pi/2$, the single-electron spin is measured. Results that would be of interest include:

- A two-qubit graph state or LU equivalent state is generated deterministically, regardless of the measurement outcome.
- A two-qubit graph state or LU equivalent state is generated probabilistically, dependent on the measurement outcome.
- The resulting two-qubit state is stabilized by generators that are weighted between a separable and maximally entangled state, similar to Eq. (5.9), where the weights are less than $\cos(\varphi)$ and greater than $\sin(\varphi)$ respectively

so that the measurement has performed some form of 'refinement' and the generated state is more entangled than the state produced when a single photon interacts with the spin.

5.4 Measurement of the Single-Electron Spin

To establish which measurement should be performed on the single-electron spin, consider a general single-qubit measurement. The basis for such a measurement is

$$\left\{ \cos(\alpha/2)\left|\uparrow\right\rangle + e^{i\beta}\sin(\alpha/2)\left|\downarrow\right\rangle,\ e^{-i\beta}\sin(\alpha/2)\left|\uparrow\right\rangle - \cos(\alpha/2)\left|\downarrow\right\rangle \right\}, \tag{5.12}$$

where $0 \leq \alpha \leq \pi$ and $0 \leq \beta < 2\pi$. The first state corresponds to measurement outcome 0 and the second to outcome 1. These states are a transformation of the computational basis states for $\mathcal{H}_s$; $A\left|\uparrow\right\rangle = \cos(\alpha/2)\left|\uparrow\right\rangle + e^{i\beta}\sin(\alpha/2)\left|\downarrow\right\rangle$ and $A\left|\downarrow\right\rangle = e^{-i\beta}\sin(\alpha/2)\left|\uparrow\right\rangle - \cos(\alpha/2)\left|\downarrow\right\rangle$, where A is the unitary and Hermitian matrix

$$A = \begin{pmatrix} \cos(\alpha/2) & e^{-i\beta}\sin(\alpha/2) \\ e^{i\beta}\sin(\alpha/2) & -\cos(\alpha/2) \end{pmatrix}. \tag{5.13}$$

Since the computational basis states have stabilizer generators $\pm Z_s$, the stabilizer generators for the basis in Eq. (5.12) are $\pm S_A$ where

$$S_A = AZ_sA^\dagger = \begin{pmatrix} \cos(\alpha) & e^{-i\beta}\sin(\alpha) \\ e^{i\beta}\sin(\alpha) & -\cos(\alpha) \end{pmatrix}. \tag{5.14}$$

This notation allows for measurement operators to be defined as

$$\begin{aligned} M_0 &= \mathbb{I}_{p_1} \otimes \mathbb{I}_{p_2} \otimes \frac{\mathbb{I}_s + S_A}{2} \\ M_1 &= \mathbb{I}_{p_1} \otimes \mathbb{I}_{p_2} \otimes \frac{\mathbb{I}_s - S_A}{2}, \end{aligned} \tag{5.15}$$

corresponding to measurement outcomes 0 and 1.

The measurement is performed on the single-electron spin, which collapses into the relevant basis state dependent on the outcome. Outcome 0 occurs with probability $p^{(0)} = [1 + \sin(\alpha)\cos(\beta)\cos^2(\varphi)]/2$ and leaves the remaining two photons in the state

$$\begin{aligned} \left|\psi\right\rangle_{p_1p_2}^{(0)} = \frac{1}{2\sqrt{2p^{(0)}}}[&(e^{2i\varphi}\cos(\alpha/2) + e^{-i\beta}\sin(\alpha/2))\left|LL\right\rangle \\ &+ e^{i\varphi}(\cos(\alpha/2) + e^{-i\beta}\sin(\alpha/2))(\left|LR\right\rangle + \left|RL\right\rangle) \\ &+ (\cos(\alpha/2) + e^{2i\varphi}e^{-i\beta}\sin(\alpha/2))\left|RR\right\rangle]. \end{aligned} \tag{5.16}$$

Similarly, outcome 1 occurs with probability $p^{(1)} = [1 - \sin(\alpha)\cos(\beta)\cos^2(\varphi)]/2$ and leaves the remaining two photons in the state

$$\begin{aligned} |\psi\rangle^{(1)}_{p_1p_2} = \frac{1}{2\sqrt{2p^{(1)}}}[&(e^{2i\varphi}e^{i\beta}\sin(\alpha/2) - \cos(\alpha/2))\,|LL\rangle \\ &+ e^{i\varphi}(e^{i\beta}\sin(\alpha/2) - \cos(\alpha/2))\,|LR\rangle + |RL\rangle) \\ &+ (e^{i\beta}\sin(\alpha/2) - e^{2i\varphi}\cos(\alpha/2))\,|RR\rangle]. \end{aligned} \tag{5.17}$$

Concurrence is used as a measure to determine the entanglement of both possible remaining states of two photons and can be calculated using Eq. (2.35). For the respective outcomes of 0 and 1, the concurrence is

$$\begin{aligned} \mathcal{C}_0 &= \frac{|\sin\alpha|\sin^2\varphi}{1 + \sin\alpha\cos\beta\cos^2(\varphi)}, \\ \mathcal{C}_1 &= \frac{|\sin\alpha|\sin^2\varphi}{1 - \sin\alpha\cos\beta\cos^2(\varphi)}. \end{aligned} \tag{5.18}$$

The aim of the single-qubit measurement is to produce a maximally entangled graph state (or LU equivalent state) between the two photons, which would have a concurrence value of 1. For fixed φ, $\mathcal{C}_0$ is maximised when $|\sin(\alpha)| = 1$ and $\sin(\alpha)\cos(\beta) = -1$, and $\mathcal{C}_1$ is maximised when $|\sin(\alpha)| = 1$ and $\sin(\alpha)\cos(\beta) = 1$. These are incompatible so the concurrence can only be maximised for one outcome. Choosing to maximise $\mathcal{C}_1$ subject to the constraint $0 \leq \alpha \leq \pi$ requires $\alpha = \pi/2$. Therefore $\cos(\beta) = 1$, requiring $\beta = 0$. Substituting these values into Eq. (5.12) gives a measurement basis

$$\left\{\frac{(|\uparrow\rangle + |\downarrow\rangle)}{\sqrt{2}}, \frac{(|\uparrow\rangle - |\downarrow\rangle)}{\sqrt{2}}\right\}, \tag{5.19}$$

which corresponds to a measurement in the X_s basis. Further substituting the values for α and β into Eq. (5.14) gives stabilizer generators $\pm X_s$ for the spin following the measurement, as expected for a measurement in the X_s basis. If instead $\mathcal{C}_0$ were maximised, the measurement would be in the $-X_s$ basis; effectively the same measurement with eigenvalues and outcomes reversed.

5.5 An X_s direction Measurement

The single-electron spin is measured in the X_s basis. Outcome 0 occurs with probability $p^{(0)} = 1 - \sin^2(\varphi)/2$ and results in the state

$$|\psi\rangle^{(0)}_{p_1p_2} = \frac{1}{\sqrt{2(1 + \cos^2(\varphi))}}[\cos(\varphi)\,|LL\rangle + |LR\rangle + |RL\rangle + \cos(\varphi)\,|RR\rangle], \tag{5.20}$$

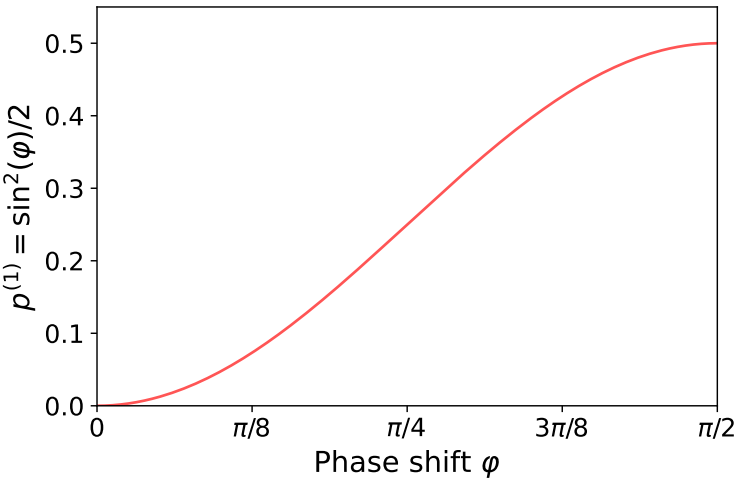

Figure 5.2: The probability of producing a heralded Bell state depending on the phase shift φ induced when two photons interact with a single-electron spin within a cavity followed by a Pauli X measurement of the spin.

with concurrence $\mathcal{C}_0 = \sin^2(\varphi)/(1+\cos^2(\varphi))$, which is less than 1 for $0 < \varphi < \pi/2$. This state is not LU equivalent to a graph state, meaning that the scheme does not succeed when the measurement outcome is 0.

Outcome 1 occurs with probability $p^{(1)} = \sin^2(\varphi)/2$ and results in the state

$$|\psi\rangle^{(1)}_{p_1p_2} = |\Phi^-\rangle = \frac{1}{\sqrt{2}}[|LL\rangle - |RR\rangle] = |\Phi^-\rangle\,, \tag{5.21}$$

with concurrence $\mathcal{C}_1 = 1$ as expected. This is a Bell state, which is LU to the two qubit graph state. This demonstrates that the spin-photon interactions and subsequent measurement can be used probabilistically as a heralded Bell state source when $\varphi < \pi/2$. However, the probability of success, $p^{(1)} = \sin^2(\varphi)/2$, as shown in Fig. 5.2, is always less than $1/2$ and decreases drastically as the angle of the induced phase shift reduces.

In the stabilizer formalism, the Bell state $|\Phi^-\rangle$ has known stabilizer generators $-X_{p_1}X_{p_2}$ and $Z_{p_1}Z_{p_2}$. Though not a stabilizer state, operators that stabilize the state can still be found for $|\psi\rangle^{(0)}_{p_1p_2}$, which can be written as a linear combination of Bell states

$$|\psi\rangle^{(0)}_{p_1p_2} = \frac{1}{\sqrt{1+\cos^2(\varphi)}}[\cos(\varphi)\,|\Phi^+\rangle + |\Psi^+\rangle]. \tag{5.22}$$

This two photon state is equivalent to applying the unitary transformation

$$\frac{1}{\sqrt{1+\cos^2(\varphi)}}[\cos(\varphi)Z_{p_1} + X_{p_1}Z_{p_2}] \tag{5.23}$$

to the Bell state $|\Phi^-\rangle$. Applying this transformation to the known generators of $|\Phi^-\rangle$ gives the stabilizer generators for $|\psi\rangle^{(0)}_{p_1p_2}$:

$$\begin{gathered} X_{p_1}X_{p_2}, \\ \frac{1}{1+\cos^2(\varphi)}[2\cos(\varphi)X_{p_1} - \sin^2(\varphi)Z_{p_1}Z_{p_2}]. \end{gathered} \tag{5.24}$$

However, these generators are not unique. The transformation on the Bell state could also be applied with photon labels reversed, resulting in stabilizer generators with reversed labels.

It is interesting to note that the scheme begins with a stabilizer state (albeit with no entanglement), then applies a non-Clifford operator followed by a Pauli measurement and, in the case of outcome 1, returns to a stabilizer state. When performing a Pauli measurement on a stabilizer state, the resulting stabilizer generators are found by manipulating existing stabilizer elements and the updated generator for the measured qubit. In this case, the single-electron spin measurement is Pauli, and an attempt to use this rule can be made despite the state before the measurement not being a stabilizer state.

Prior to the measurement, the full stabilizer is found by multiplying together the generators in Eq. (5.10):

$$\begin{gathered} \mathbb{I} \\ X_{p_1}\cos(\varphi) - Y_{p_1}Z_s\sin(\varphi) \\ X_{p_2}\cos(\varphi) - Y_{p_2}Z_s\sin(\varphi) \\ X_s\cos^2(\varphi) - (Z_{p_1}Y_s + Z_{p_2}Y_s)\sin(\varphi)\cos(\varphi) - Z_{p_1}Z_{p_2}X_s\sin^2(\varphi) \\ X_{p_1}X_s\cos(\varphi) - X_{p_1}Z_{p_2}Y_s\sin(\varphi) \\ X_{p_2}X_s\cos(\varphi) - Z_{p_1}X_{p_2}Y_s\sin(\varphi) \\ X_{p_1}X_{p_2}\cos^2(\varphi) - (Y_{p_1}X_{p_2}Z_s + X_{p_1}Y_{p_2}Z_s)\sin(\varphi)\cos(\varphi) + Y_{p_1}Y_{p_2}\sin^2(\varphi) \\ X_{p_1}X_{p_2}X_s \end{gathered} \tag{5.25}$$

The measured qubit has stabilizer generator $\pm X_s$ depending on the measurement outcome. Multiplying the final element of the stabilizer $X_{p_1}X_{p_2}X_s$ by $\pm X_s$ gives $\pm X_{p_1}X_{p_2}$, which is one of the stabilizer generators for the state following the measurement. This is the only generator that commutes with $\pm X_s$ and the second stabilizer generator for either outcome cannot be found by manipulation of the stabilizer elements. It is unclear why this is the case, though is likely due to the

state following the interaction not being a true stabilizer state. Returning to the general measurement, with stabilizer generators $\pm S_A$, it is also not apparent how stabilizer generators for the remaining states of two photons would be found, as again, manipulation of stabilizer generators in the manner of a Pauli measurement of a graph state does not appear to work and in general, $\pm S_A$ will not commute with the existing generators.

5.6 Generating Larger Photonic Graph States

The interaction and subsequent measurement of the single-electron spin can be used to entangle photon pairs and can be extended to produce larger photonic graph states. Such a scheme has two 'layers' as shown in Fig. 5.3, where the first layer is used to entangle photon pairs and the second connects these entangled pairs. The steps to enact the scheme are as follows:

First Layer

- Single photons are prepared in the state $|+\rangle_p$. Single-electron spins contained within cavities are prepared in the state $|+\rangle_s$.
- A pair of photons is sent into every cavity within the first layer to interact with the single-electron spin. The electron spin in each of these cavities is measured in the X_s direction.
- For measurements with outcome 1, a Bell state is produced and the pair of photons is retained.
- For measurements with outcome 0, the photons are discarded as the state produced is not seen as useful.
- A minimum requirement for storage of the photons is the time it takes to perform the X_s direction measurements and process the outcomes. However if the produced Bell pairs can be stored in a quantum memory for a longer duration then further steps can be taken for cavities where the outcome is 0. The state of the electron spin in each cavity where this is the case returns to $|+\rangle_s$, as it was initially set-up to be. The procedure of sending in two photons and performing an X_s measurement can be repeated until a sufficient number of Bell states have been produced.

Second Layer

- The photons are paired with a photon from another Bell state (with the exception of the first and final photons as shown in Fig. 5.3).

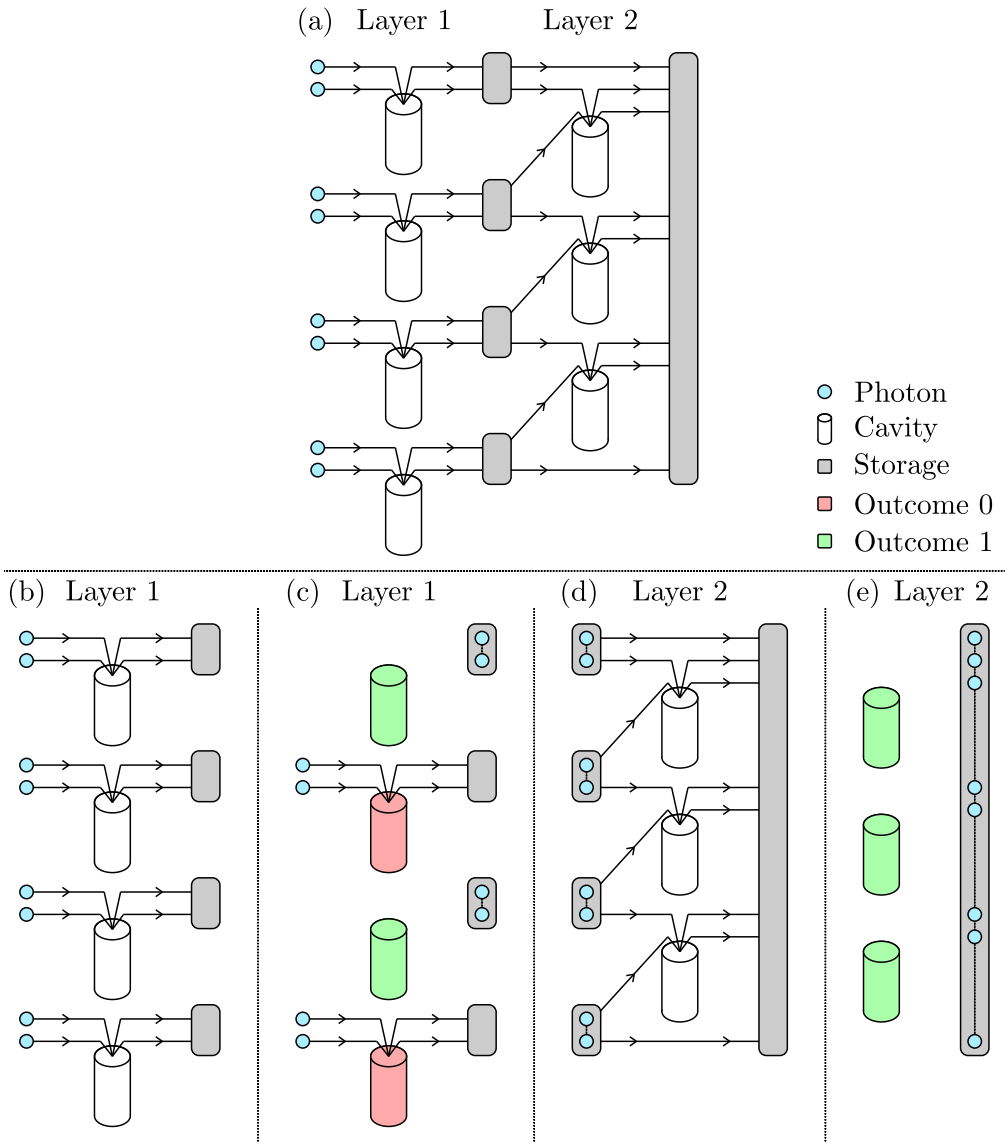

Figure 5.3: A two layer scheme to generate photonic GHZ style states. (a) An overview of the scheme showing the set-up and routing. (b) A pair of single photons is sent in sequentially to each cavity in the first layer to interact with single-electron spins. (c) The single-electron spins are measured in the X_s direction with outcome 1 leading to Bell states being stored whilst the previous step is repeated for outcome 0 with further photons sent into the cavities. (d) Photons from the stored Bell states are paired up and sent into the second layer cavities, excluding the first and final photons. (e) The single-electron spins in the second layer are measured in the X_s direction and, provided all outcomes are 1, a large photonic GHZ style state is produced.

- The new photon pairs pass into the cavities in the second layer and interact with the single-electron spins, which are subsequently measured in the X_s basis.

- In order for the procedure to succeed, all measurement outcomes must be 1 within the second layer. The probability of this is

$$\prod_{i=1}^{n_s^{(2)}} \frac{1}{2} \sin^2(\varphi_i). \tag{5.26}$$

  where $n_s^{(2)}$ is the number of single-electron spins in the second layer and each φ_i is the phase shift induced the relevant cavity, which need not be equal.

- When the scheme succeeds, the resulting state of $n_p = 2(n_s^{(2)} + 1)$ photons is

$$\frac{|L\rangle^{\otimes n_p} - |R\rangle^{\otimes n_p}}{\sqrt{2}}. \tag{5.27}$$

  This is a GHZ state with a phase flip applied.

It is also possible to entangle an odd number of photons. An extra photon is prepared in the state $|+\rangle_p$ and sent into an additional cavity in the second layer alongside the final photon. Again, the X_s basis measurements of all $n_s^{(2)}$ single-electron spins in the second layer must have outcome 1. This produces the GHZ state

$$\frac{|L\rangle^{\otimes n_p} + |R\rangle^{\otimes n_p}}{\sqrt{2}}, \tag{5.28}$$

where $n_p = 2n_s^{(2)} + 1$ is the number of photons in the state.

To demonstrate the low probability of success, consider the case in which each cavity within the second layer induces an identical phase shift of φ. The probability of all measurement outcomes being 1 is

$$\left(\frac{1}{2} \sin^2(\varphi)\right)^{n_s^{(2)}}. \tag{5.29}$$

Since $0 < \sin^2(\varphi) < 1$ for $0 < \varphi < \pi/2$ this probability is bounded above by $2^{-n_s^{(2)}}$, which decreases exponentially as the number of spins within the second layer increases. Fig. 5.4 shows this success probability for a second layer consisting of 1 to 6 cavities containing an electron spin.

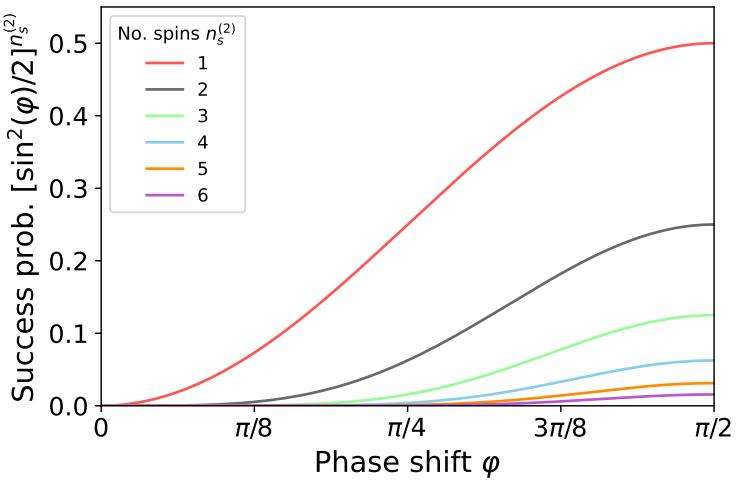

Figure 5.4: The probability of all measurement outcomes in layer 2 being 1 and the scheme producing a GHZ-style state for a second layer ranging from 1 to 6 single-electron spins.

5.7 Discussion

We have demonstrated that the interaction between photons and a single-electron spin can be utilised as a means to generate stabilizer states probabilistically even when the phase shift induced by the interaction is small, i.e. $\varphi < \pi/2$. In the simplest case, where two photons interact with the spin, followed by measurement of the spin, the process acts as a probabilistic heralded Bell state source, which is an important resource for quantum computing. When the scheme is enacted on a larger scale with multiple cavities, larger photonic GHZ style states can be produced, albeit with a low probability of success.

Though the stabilizer formalism is used as a means to track the interaction of photons with the cavity, it is not possible to manipulate the generators once a measurement in the X_s basis is performed. Further work could determine why only one stabilizer generator is found for each measurement outcome, especially in the case where the measurement outcome is 1, as the remaining Bell state is a stabilizer state and is readily described by stabilizer generators. This could also be extended to an investigation of the stabilizer generators $\pm S_A$ and potential generators for a remaining state following a more general measurement of the single-electron spin.

Future investigation could consider whether distillation could be used to produce Bell pairs from the remaining state of two photons when the measurement outcome is 0. A protocol such as BBPSSW [27] or DEJMPS [28] requires mul-

tiple copies of the state to be distilled and is itself probabilistic, meaning that the resources required to recover Bell pairs in this way may not be more effective than using the spin-photon interaction and requiring the measurement outcome 1, despite the probability of this outcome being small. Additional work surrounding the larger layered scheme could examine whether some form of distillation or refinement could be applied to produce a 'useful' photonic graph state when one or more of the measurement outcomes is 0, or to study whether a different structure could lead to another LU class of graph states.

Chapter 6

Summary

The work presented in this thesis focused on graph states and their importance as an entangled resource within quantum computation and communication in applications ranging from MBQC to quantum repeaters. Despite their perceived simplicity in having a visual representation consisting only of vertices and edges, graph states allow access to a highly entangled class of quantum states, and have a powerful mathematical 'language' — the stabilizer formalism.

We began this thesis by discussing the role of graph states within quantum information applications and how the stabilizer formalism ties to their description despite being initially developed for QEC. In Chapter 2 we presented the mathematical toolkit necessary to describe graph states, states resulting from their manipulation, and the specific quantum concept of entanglement. Following this we addressed three distinct uses of the stabilizer formalism to look at properties, operation with and generation of graph states.

Chapter 3 mapped the number of sets of stabilizer generators describing a reduced graph state to the purity of the remaining state. This result allows for efficient calculation of the entanglement measure Concentratable Entanglement for graph states when its definition is given in terms of these purities. We applied this to several example graph states including 'snowflake states' that have been designed for quantum repeaters and all graph states containing up to nine qubits.

In Chapter 4 we investigated MBQC for the specific task of implementing a two-qubit unitary. We provided a step-by-step derivation of the protocol starting with the translation of each of the necessary gates from a circuit based model to the measurement based set-up. We reduced the number of qubits within the graph state resource by theoretically performing the Pauli measurements and tracking the adjustments and byproduct operators required.

Lastly, in Chapter 5 we studied interactions between photons and electron spins within quantum dots as a means to generate graph states in the case where the induced phase shift was $\varphi < \pi/2$. We showed that this set-up led to the

probabilistic generation of Bell pairs, heralded by measurement of the electron spin and, when repeated on a larger scale with multiple cavities and photons, the scheme could be used to produce GHZ style states.

Chapters 3 and 4 demonstrate the efficiency with which the stabilizer formalism can be used to describe and manipulate graph states when operations consist of Clifford group operations and Pauli measurements, as required by the Gottesman-Knill Theorem. However, Chapter 5 highlights the complications that arise when operations are applied beyond this restriction and how the group structure of the stabilizer can no longer be used to track states resulting from a subsequent measurement, even though it is possible for the final state to be a stabilizer state.

Future work relating to Chapter 3 could consider whether the use of the stabilizer formalism to calculate Concentratable Entanglement could be extended to graph states of qudits, hypergraph states or graph states where an error occurs, resulting in a mixed state. Each of these would increase the number of sets of stabilizer generators that describe the state either before or after tracing out qubits (or qudits) to find the reduced state purities, and this number may no longer correspond to the purities required.

Perhaps most interesting from a practical or experimentalist viewpoint is the work of Chapter 4, as progress is already being made by members of QET Labs in Bristol on designing the set-up to produce the adapted graph state and to implement the protocol on-chip. To make the two-qubit unitary as general as possible, the local operations u_1, v_1, u_4 and v_4 could also be included within the MBQC protocol, though this would increase the number of qubits within the resource graph state, which may be too large to produce by those in Bristol as it stands.

Further extension on the work of Chapter 5 would likely focus on distillation of Bell states or larger GHZ style states in cases where the scheme is considered a failure when the measurement outcome is 0. This is unlikely to require the stabilizer formalism, as the resulting states in this scenario are not stabilizer states and it would be inefficient to track stabilizer generators. However this may be more resource intensive than the proposed probabilistic scheme, as the distillation process may be less likely to succeed or require multiple rounds to produce a state with high fidelity.

Bibliography

[1] A. Peruzzo, J. McClean, P. Shadbolt, M.-H. Yung, X.-Q. Zhou, P. J. Love, A. Aspuru-Guzik, and J. L. O'Brien, Nat. Commun. **5**, 4213 (2014).

[2] J. Tilly, H. Chen, S. Cao, D. Picozzi, K. Setia, Y. Li, E. Grant, L. Wossnig, I. Rungger, G. H. Booth, and J. Tennyson, Phys. Rep. **986**, 1–128 (2022).

[3] L. K. Grover, in *STOC '96: Proceedings of the Twenty-Eighth Annual ACM Symposium on Theory of Computing* (1996) p. 212–219.

[4] P. Shor, in *Proceedings 35th Annual Symposium on Foundations of Computer Science* (1994) pp. 124–134.

[5] J. Biamonte, P. Wittek, N. Pancotti, P. Rebentrost, N. Wiebe, and S. Lloyd, Nature **549**, 195–202 (2017).

[6] V. Dunjko, J. M. Taylor, and H. J. Briegel, Phys. Rev. Lett. **117**, 130501 (2016).

[7] N. Wiebe, A. Kapoor, and K. M. Svore, "Quantum perceptron models," (2016), arXiv:1602.04799 .

[8] S. Lloyd, M. Mohseni, and P. Rebentrost, Nat. Phys. **10**, 631–633 (2014).

[9] P. Rebentrost, M. Mohseni, and S. Lloyd, Phys. Rev. Lett. **113**, 130503 (2014).

[10] C. H. Bennett, G. Brassard, and J.-M. Robert, SIAM J. Comput. **17**, 210 (1988).

[11] A. K. Ekert, Phys. Rev. Lett. **67**, 661 (1991).

[12] J. Preskill, "Quantum computing and the entanglement frontier," (2012), arXiv:1203.5813 .

[13] A. Einstein, B. Podolsky, and N. Rosen, Phys. Rev. **47**, 777 (1935).

[14] E. Schrödinger, Math. Proc. Camb. Phil. Soc. **31**, 555 (1935).

[15] R. Raussendorf and H. J. Briegel, Phys. Rev. Lett. **86**, 5188 (2001).

[16] R. Raussendorf, D. E. Browne, and H. J. Briegel, Phys. Rev. A **68**, 022312 (2003).

[17] M. Hein, J. Eisert, and H. J. Briegel, Phys. Rev. A **69**, 062311 (2004).

[18] H. J. Kimble, Nature **453**, 1023–1030 (2008).

[19] S. Wehner, D. Elkouss, and R. Hanson, Science **362**, eaam9288 (2018).

[20] J. Yin, Y. Cao, Y.-H. Li, S.-K. Liao, L. Zhang, J.-G. Ren, W.-Q. Cai, W.-Y. Liu, B. Li, H. Dai, G.-B. Li, Q.-M. Lu, Y.-H. Gong, Y. Xu, S.-L. Li, F.-Z. Li, Y.-Y. Yin, Z.-Q. Jiang, M. Li, J.-J. Jia, G. Ren, D. He, Y.-L. Zhou, X.-X. Zhang, N. Wang, X. Chang, Z.-C. Zhu, N.-L. Liu, Y.-A. Chen, C.-Y. Lu, R. Shu, C.-Z. Peng, J.-Y. Wang, and J.-W. Pan, Science **356**, 1140 (2017).

[21] C. H. Bennett, G. Brassard, C. Crépeau, R. Jozsa, A. Peres, and W. K. Wootters, Phys. Rev. Lett. **70**, 1895 (1993).

[22] W. K. Wootters and W. H. Zurek, Nature **299**, 802 (1982).

[23] D. Dieks, Physics Letters A **92**, 271 (1982).

[24] H.-J. Briegel, W. Dür, J. I. Cirac, and P. Zoller, Phys. Rev. Lett. **81**, 5932 (1998).

[25] W. Dür, H.-J. Briegel, J. I. Cirac, and P. Zoller, Phys. Rev. A **59**, 169 (1999).

[26] M. Żukowski, A. Zeilinger, M. A. Horne, and A. K. Ekert, Phys. Rev. Lett. **71**, 4287 (1993).

[27] C. H. Bennett, G. Brassard, S. Popescu, B. Schumacher, J. A. Smolin, and W. K. Wootters, Phys. Rev. Lett. **76**, 722 (1996).

[28] D. Deutsch, A. Ekert, R. Jozsa, C. Macchiavello, S. Popescu, and A. Sanpera, Phys. Rev. Lett. **77**, 2818 (1996).

[29] L.-M. Duan, M. D. Lukin, J. I. Cirac, and P. Zoller, Nature **414**, 413 (2001).

[30] L. Jiang, J. M. Taylor, and M. D. Lukin, Phys. Rev. A **76**, 012301 (2007).

[31] Z.-B. Chen, B. Zhao, Y.-A. Chen, J. Schmiedmayer, and J.-W. Pan, Phys. Rev. A **76**, 022329 (2007).

[32] O. A. Collins, S. D. Jenkins, A. Kuzmich, and T. A. B. Kennedy, Phys. Rev. Lett. **98**, 060502 (2007).

[33] L. Childress, J. M. Taylor, A. S. Sørensen, and M. D. Lukin, Phys. Rev. Lett. **96**, 070504 (2006).

[34] K. Nemoto, M. Trupke, S. J. Devitt, B. Scharfenberger, K. Buczak, J. Schmiedmayer, and W. J. Munro, Sci Rep **6**, 26284 (2016).

[35] S. E. Vinay and P. Kok, Phys. Rev. A **95**, 052336 (2017).

[36] M. Zwerger, W. Dür, and H. J. Briegel, Phys. Rev. A **85**, 062326 (2012).

[37] K. Azuma, K. Tamaki, and H.-K. Lo, Nat. Commun. **6**, 6787 (2015).

[38] P. W. Shor, Phys. Rev. A **52**, R2493 (1995).

[39] A. M. Steane, Phys. Rev. Lett. **77**, 793 (1996).

[40] D. Gottesman, "Stabilizer Codes and Quantum Error Correction," (1997), arxiv:quant-ph/9705052 .

[41] J. L. Beckey, N. Gigena, P. J. Coles, and M. Cerezo, Phys. Rev. Lett. **127**, 140501 (2021).

[42] C. Y. Hu, A. Young, J. L. O'Brien, W. J. Munro, and J. G. Rarity, Phys. Rev. B **78**, 085307 (2008).

[43] C. Y. Hu, W. J. Munro, and J. G. Rarity, Phys. Rev. B **78**, 125318 (2008).

[44] J. von Neumann, *Mathematical Foundations of Quantum Mechanics*, New ed. (Princeton University Press, 2018).

[45] D. Gottesman, in *Group22: Proceedings of the XXII International Colloquium on Group Theoretical Methods in Physics,* (1999) pp. 32–43.

[46] J. Roffe, Contemporary Physics **60**, 226 (2019).

[47] D. Schlingemann and R. F. Werner, Phys. Rev. A **65**, 012308 (2001).

[48] M. Grassl, A. Klappenecker, and M. Roetteler, in *Proceedings IEEE International Symposium on Information Theory,* (2002) p. 45.

[49] P. Kok and B. W. Lovett, *Introduction to Optical Quantum Information Processing* (Cambridge University Press, 2010).

[50] R. Horodecki, P. Horodecki, M. Horodecki, and K. Horodecki, Rev. Mod. Phys. **81**, 865 (2009).

[51] C. H. Bennett, D. P. DiVincenzo, J. A. Smolin, and W. K. Wootters, Phys. Rev. A **54**, 3824 (1996).

[52] V. Vedral, M. B. Plenio, M. A. Rippin, and P. L. Knight, Phys. Rev. Lett. **78**, 2275 (1997).

[53] G. Vidal, J. Mod. Opt. **47**, 355 (2000).

[54] S. Hill and W. K. Wootters, Phys. Rev. Lett. **78**, 5022 (1997).

[55] W. K. Wootters, Phys. Rev. Lett. **80**, 2245 (1998).

[56] P. Rungta, V. Bužek, C. M. Caves, M. Hillery, and G. J. Milburn, Phys. Rev. A **64**, 042315 (2001).

[57] W. Dür, G. Vidal, and J. I. Cirac, Phys. Rev. A **62**, 062314 (2000).

[58] D. A. Meyer and N. R. Wallach, J. Math. Phys. **43**, 4273 (2002).

[59] G. Brennen, Quantum Inf. Comput. **3**, 619 (2003).

[60] A. R. R. Carvalho, F. Mintert, and A. Buchleitner, Phys. Rev. Lett. **93**, 230501 (2004).

[61] D. M. Greenberger, M. A. Horne, and A. Zeilinger, in *Bell's Theorem, Quantum Theory, and Conceptions of the Universe* (1989) pp. 69–72.

[62] N. D. Mermin, Am. J. Phys **58**, 731 (1990).

[63] M. Van den Nest, J. Dehaene, and B. De Moor, Phys. Rev. A **71**, 062323 (2005).

[64] H. J. Briegel, D. E. Browne, W. Dür, R. Raussendorf, and M. V. den Nest, Nature Phys **5**, 19 (2009).

[65] D. Markham and B. C. Sanders, Phys. Rev. A **78**, 042309 (2008).

[66] S. Foulds, V. Kendon, and T. Spiller, Quantum Science and Technology **6**, 035002 (2021).

[67] A. Wong and N. Christensen, Phys. Rev. A **63**, 044301 (2001).

[68] M. Hein, W. Dür, J. Eisert, R. Raussendorf, M. V. den Nest, and H.-J. Briegel, in *Proceedings of the International School of Physics "Enrico Fermi" on "Quantum Computers, Algorithms and Chaos"* (2006) pp. 115–218.

[69] A. R. Cullen and P. Kok, Phys. Rev. A **106**, 042411 (2022).

[70] H. Buhrman, R. Cleve, J. Watrous, and R. de Wolf, Phys. Rev. Lett. **87**, 167902 (2001).

[71] M. Nielsen and I. Chuang, *Quantum Computation and Quantum Information*, 10th ed. (Cambridge University Press, 2010).

[72] L. E. Danielsen and M. G. Parker, J. Comb. Theory, Series A **113**, 1351 (2006).

[73] A. Cabello, L. E. Danielsen, A. J. López-Tarrida, and J. R. Portillo, Phys. Rev. A **83**, 042314 (2011).

[74] W. Helwig, W. Cui, A. Riera, J. I. Latorre, and H.-K. Lo, Phys. Rev. A **86**, 052335 (2012).

[75] I. Schwartz, D. Cogan, E. R. Schmidgall, Y. Don, L. Gantz, O. Kenneth, N. H. Lindner, and D. Gershoni, Science **354**, 434 (2016).

[76] D. Istrati, Y. Pilnyak, J. C. Loredo, C. Antón, N. Somaschi, P. Hilaire, H. Ollivier, M. Esmann, L. Cohen, L. Vidro, C. Millet, A. Lemaître, I. Sagnes, A. Harouri, L. Lanco, P. Senellart, and H. S. Eisenberg, Nat. Commun. **11**, 5501 (2020).

[77] A. Hagberg, P. Swart, and D. Schult, in *Proceedings of the 7th Python in Science Conference* (2008) pp. 11–15.

[78] B. McKay, "Graphs," `https://users.cecs.anu.edu.au/~bdm/data/graphs.html`, [Online; Accessed 27 Apr 2022].

[79] S. Foulds, O. Prove, and V. Kendon, Phil. Trans. R. Soc. A **382**, 20240411 (2024).

[80] S. Y. Looi, L. Yu, V. Gheorghiu, and R. B. Griffiths, Phys. Rev. A **78**, 042303 (2008).

[81] A. Keet, B. Fortescue, D. Markham, and B. C. Sanders, Phys. Rev. A **82**, 062315 (2010).

[82] W. Helwig, "Absolutely Maximally Entangled Qudit Graph States," (2013), arxiv:1306.2879 .

[83] M. Rossi, M. Huber, D. Bruß, and C. Macchiavello, New J. Phys. **15**, 113022 (2013).

[84] R. Qu, J. Wang, Z.-s. Li, and Y.-r. Bao, Phys. Rev. A **87**, 022311 (2013).

[85] F. E. S. Steinhoff, C. Ritz, N. I. Miklin, and O. Gühne, Phys. Rev. A **95**, 052340 (2017).

[86] J. L. Beckey, G. Pelegrí, S. Foulds, and N. J. Pearson, Phys. Rev. A **107**, 062425 (2023).

[87] G. Vidal and C. M. Dawson, Phys. Rev. A **69**, 010301 (2004).

[88] M. W. Coffey, R. Deiotte, and T. Semi, Phys. Rev. A **77**, 066301 (2008).

[89] M. A. Nielsen, Rep. Math. Phys. **57**, 147–161 (2006).

[90] X. Zhou, D. W. Leung, and I. L. Chuang, Phys. Rev. A **62**, 052316 (2000).

[91] D. E. Browne and H. J. Briegel, "One-way Quantum Computation - a tutorial introduction," (2006), arxiv:quant-ph/0603226 .

[92] L.-M. Duan and H. J. Kimble, Phys. Rev. Lett. **92**, 127902 (2004).

[93] C. Y. Hu and J. G. Rarity, Phys. Rev. B **83**, 115303 (2011).

[94] E. Callus and P. Kok, Phys. Rev. A **108**, 042613 (2023).